UNCLASSIFIED

AD 463575

DEFENSE DOCUMENTATION CENTER

FOR

SCIENTIFIC AND TECHNICAL INFORMATION

CAMERON STATION ALEXANDRIA, VIRGINIA

UNCLASSIFIED

NOTICE: When government or other drawings, specifications or other data are used for any purpose other than in connection with a definitely related government procurement operation, the U. S. Government thereby incurs no responsibility, nor any obligation whatsoever; and the fact that the Government may have formulated, furnished, or in any way supplied the said drawings, specifications, or other data is not to be regarded by implication or otherwise as in any manner licensing the holder or any other person or corporation, or conveying any rights or permission to manufacture, use or sell any patented invention that may in any way be related thereto.

Department of

MECHANICAL ENGINEERING

of

THE UNIVERSITY OF MARYLAND

An Experimental Study of the Effects of Boundary Layer Thickness and Velocity Profile on the Pressure Distributions of Objects Immersed in the Boundary Layer

by

Clifford L. Sayre, Jr.

Unclassified

February 1965

Report No. M.E.595(19)
Mechanical Engineering Dept.
University of Maryland

ONR Contract Nonr 595(19)

TABLE of CONTENTS

LIST of TABLES

LIST of ILLUSTRATIONS

NOTATION

C_p	Pressure coefficient (Equation 1, page 4)
C_{pmin}	Minimum pressure coefficient
D	Diameter
p	Local static pressure
p_∞	Free-stream static pressure
v	Local velocity in boundary layer
V_∞	Free-stream velocity
x	Longitudinal coordinate in flow direction
y	Coordinate perpendicular to boundary
δ	Boundary layer thickness
δ^*	Displacement thickness (Equation 2, page 4)
θ	Momentum thickness (Equation 3, page 4)
ρ	Mass density

ABSTRACT

Pressure distributions were measured on six models in three different boundary layer conditions. Two hemispheres, two semicylinders, and two half bodies of revolution were used in the tests. The range of Reynolds numbers for the hemispheres and semicylinders was from 0.6×10^5 to 1.6×10^5 (based on diameter and free stream velocity). The boundary layer thicknesses ranged from about one-half to twice the characteristic model dimension. The effect of increasing boundary layer thickness (or momentum thickness) was a reduction in the positive and negative ordinates of the pressure distributions. The pressures on three- dimensional models were approximately the same at a given longitudinal station, although there may have been a small reduction in pressures close to the wall on which the object was mounted. No simple relationship could be found for relating the changes in pressure distribution to changes in velocity profile or boundary layer thickness, however a data correlation was obtained relating the minimum pressure coefficient for a particular boundary layer condition to the minimum pressure coefficient measured in a unifrom flow.

INTRODUCTION

Information concerning pressure distributions on bodies plays an important role in aerodynamics and hydrodynamics. The magnitudes of local pressures and the locations of minimum pressure points provide data for estimating the conditions for cavitation in a liquid flow or the onset of compressibility effects in a gas flow. Integration of the pressures with respect to a particular direction provides information on the lift or drag force acting on a body. Considerable effort has been devoted to the measurement of pressure distributions on bodies and to the development of methods for calculating such pressure distributions from potential flow patterns. Most of the results from such studies are applicable to the pressures experienced by a body in an initially uniform flow field. Comparatively little has been done toward measuring or developing methods for calculating pressure distributions in an initially non-uniform flow field.

One example of a body in a non-uniform flow is that of an appendage on a ship or aircraft which is partially or fully immersed in the boundary layer of the vehicle. Weighardt (1)* and Tillman (2) describe the results from drag measurement tests made on a variety of shapes immersed in various boundary layers. The forces experienced by ground mines or other objects (3) on the bottom or sides of a channel are another aspect of such flows. Holl (4) gives results from a theoretical and expermental study of the influence of boundary layer thickness and velocity profile on the cavitation number for circular arcs and wedge-shaped profiles. The present tests were undertaken to measure the influence of boundary layer thickness and velocity profile on the pressure distributions of several simple two- and three-dimensional shapes.

EXPERIMENTATION

Pressure distributions were measured on semicylinders, hemispheres, and half-models mounted on the wall of a wind tunnel having an 18" x 18" test section. The models and pressure tap locations are shown in Figures 1 and 2. Offsets for the half-models are given in Table 1. Pressures on the rear of the semicylinders were obtained by reversing the models. Pressure distributions on the surface of the hemispheres were obtained by rotating the models about the axis of symmetry. The nominal tunnel free-stream velocity for all of the tests was 75 feet per second. Pressures were measured on a slanted, multiple-tube manometer board which was calibrated against a micromanometer. The pressure readings have been converted to conventional pressure coefficients based on free-stream static and dynamic pressures

*Numbers in parentheses refer to the list of references.

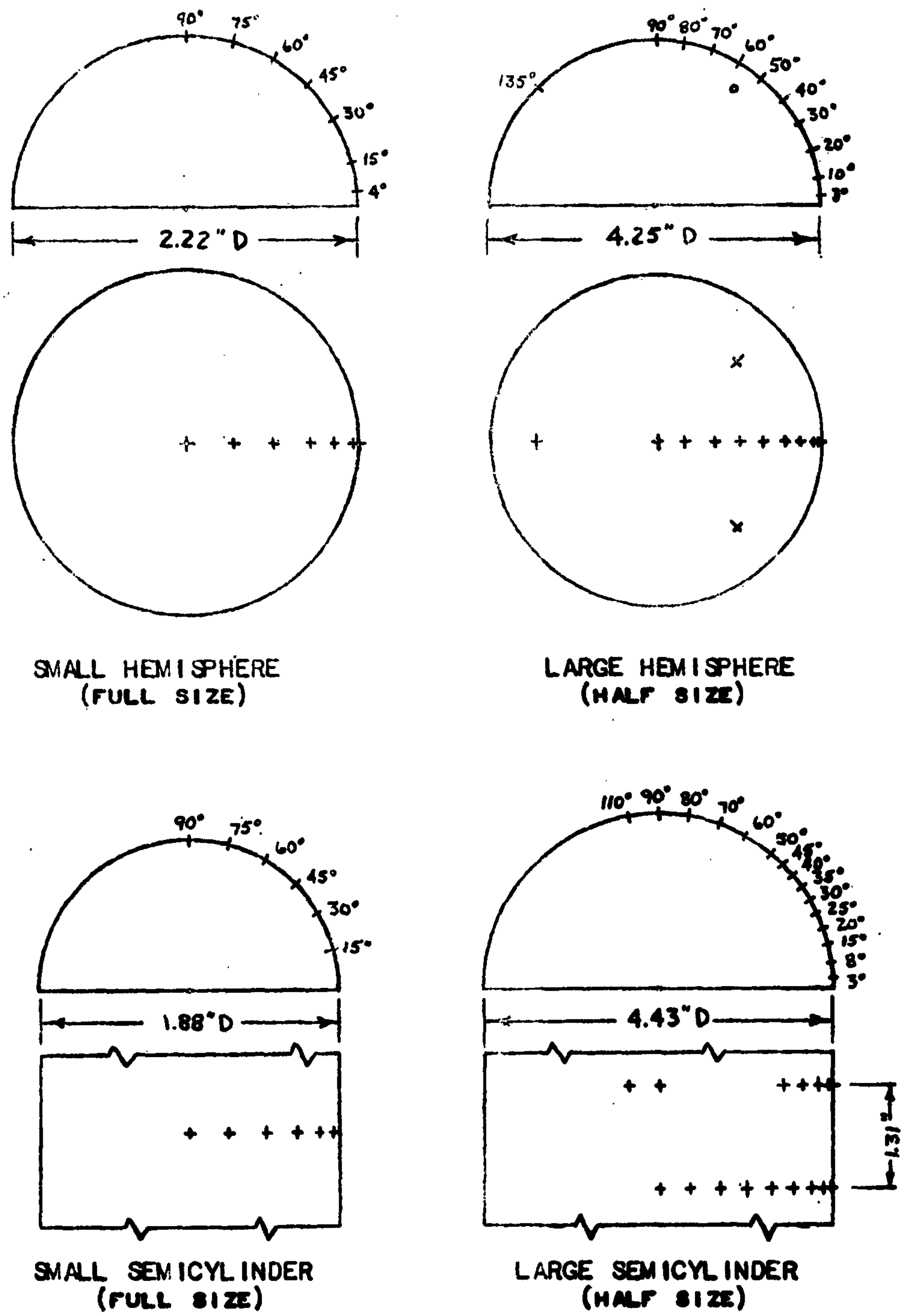

FIGURE 1 - MODEL HEMISPHERE AND SEMICYLINDER GEOMETRY
(+ STATIC PRESSURE ORIFICE LOCATIONS)

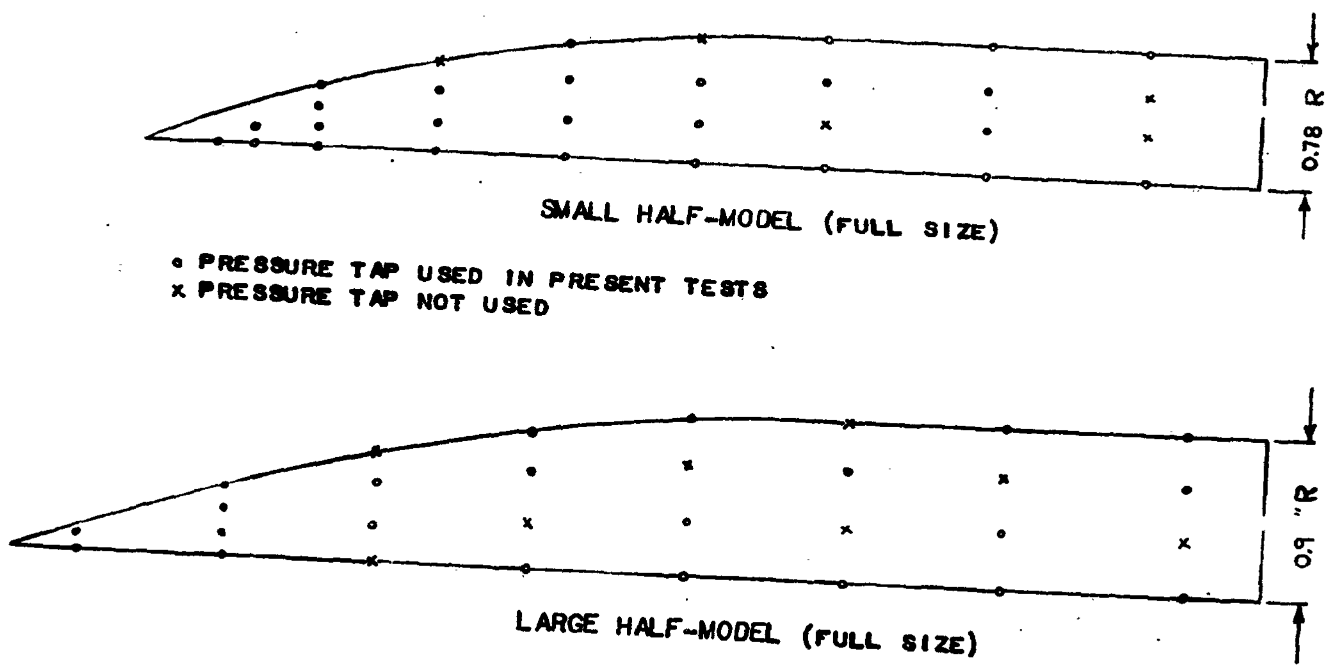

FIGURE 2 - HALF-MODEL GEOMETRY

$$C_p = \frac{p - p_\infty}{\frac{\rho}{2} V_\infty^2} \tag{1}$$

Two sizes of semicylinders and hemispheres were used to give some relative changes in model and boundary layer proportions without requiring changes in boundary layer properties. The hemispheres and half-models were also tested away from the wall to determine the pressure distributions in a uniform flow.

One natural and two simulated boundary layers were used for the tests. The natural boundary layer profile was that normally existing along the tunnel wall. Artificial boundary or shear layers were created by stringing 0.0175" diameter monofilament nylon fishing line in patterns upstream of the models. The lines were strung from wall to wall three feet ahead of the models. The boundary layer measurements were made at the location of the model without the model in place. Figure 3 shows the boundary layer velocity profiles superimposed for comparative purposes. The individual profiles are shown in Figures 10, 11, and 12. The string patterns for the artificial boundary layers are also shown in Figures 11 and 12. Displacement thickness and momentum thickness were calculated graphically from the following definitions (5)

$$\delta^* = \int_0^\delta \left(1 - \frac{v}{V_\infty}\right) dy \tag{2}$$

$$\theta = \int_0^\delta \frac{v}{V_\infty} \left(1 - \frac{v}{V_\infty}\right) dy \tag{3}$$

Boundary layer characteristics are given in Table 2.

Figure 3 and Table 2 show that the natural boundary layer and first artificial boundary layer had approximately the same profile with the latter having twice the thickness of the former. The artificial layers were of about the same thickness but with different velocity profiles.

The following data are believed to be reasonable estimates of the precision of various parameters associated with the tests:

Models - dimensions ± 0.01 inch
angles ± 1.0 degree

Pressure coefficients (std. deviations) -
spheres and cylinders ± 0.03
half-models ± 0.01

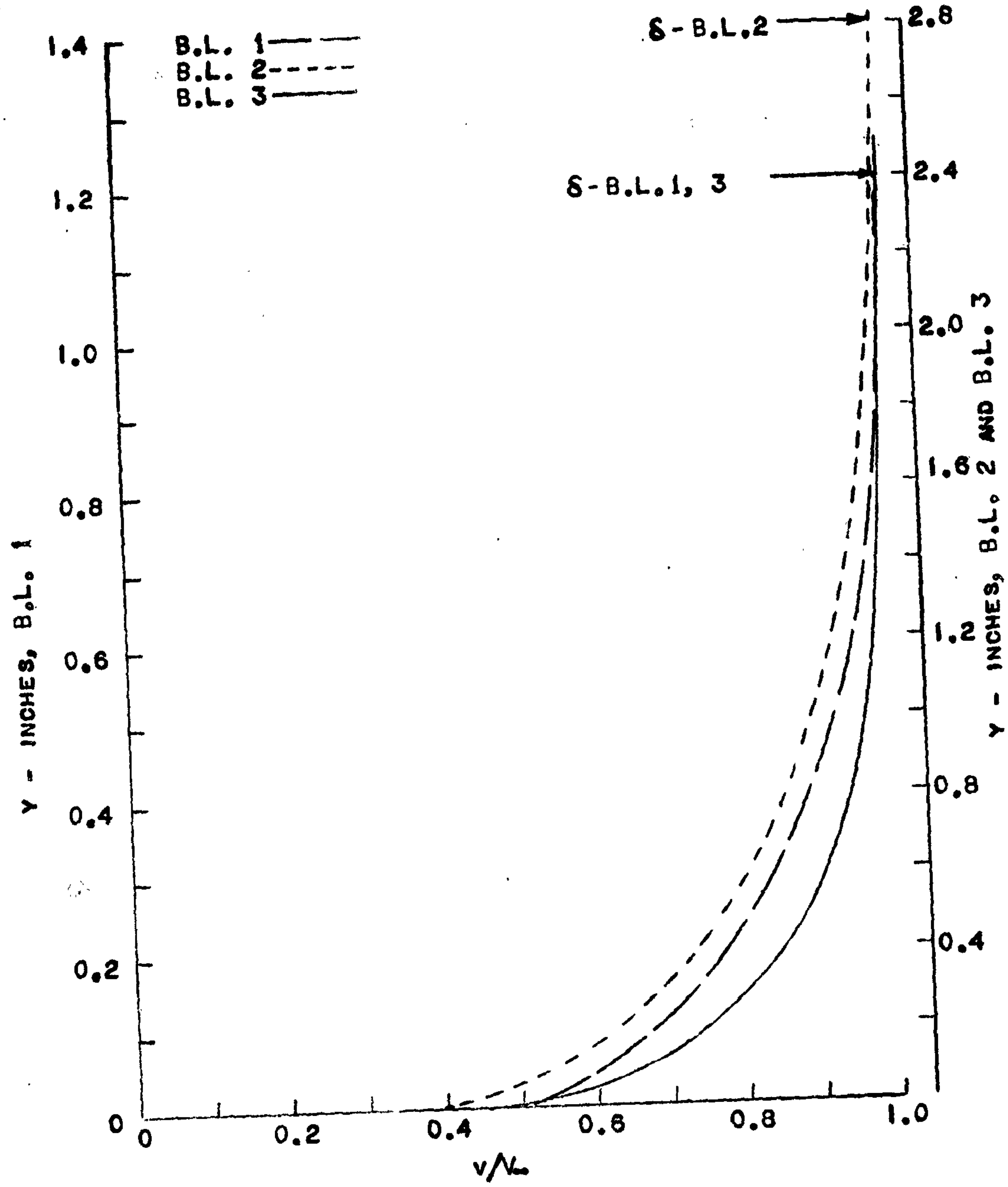

FIGURE 3 - COMPARISON OF VELOCITY PROFILES

DISCUSSION of RESULTS

Pressure distributions on the centerline of the large hemisphere for the free-stream and various boundary layer conditions are shown in Figure 4. Figures 13, 14, and 15 are separate tabulations of pressure coefficients over the surface of the hemisphere for each of the three boundary layer conditions. The various rings of readings have been separated by equal distances on the chart in order to provide room for recording the values. A true plan view would crowd the rings for small angles as illustrated by the closeness of the orifice locations shown in the plan views of the hemispheres in Figure 1.

Figure 5 shows centerline pressures for the small hemisphere. Figures 16, 17, and 18 show the pressure coefficient distributions over the surface of the small hemisphere.

A comparison of the centerline pressure distributions in Figures 4 and 5 shows a difference in free-stream results for the two hemispheres. The pressures agree up to about 60°; then the larger hemisphere reaches a lower negative value of pressure coefficient. In addition, the pressures on most of the after part of the large sphere are less negative than for the small hemisphere. Both of these factors are characteristic of pressure distributions above and below the transition point from a laminar to a turbulent boundary layer. The Reynolds numbers for the large and small sphere were 1.6×10^5 and 0.8×10^5, respectively (based on diameter). These values are in the range near the critical region where the drag coefficient changes markedly. The exact value of Reynolds number for transition depends upon the amount of turbulence in the wind tunnel stream and the roughness of the model. Figure 202 in Goldstein shows a similar variation in pressure distributions on a sphere over a range of Reynolds numbers from 1.6×10^5 to 4.2×10^5. The differences shown in the present results are attributed to similar effects above and below the transition Reynolds number. The numerical values of Reynolds numbers corresponding to the present results and those cited in Reference 6 for similar pressure distributions probably differ because of differences in the free-stream turbulence levels of the wind tunnels.

The pressure distributions shown in Figures 4 and 5 for the various boundary layer conditions are typical of the results for all models tested. In general, the positive pressures are lower (i.e., less positive) and the negative pressure coefficients are smaller (i.e., less negative) as the boundary layer thickness increases. It would be more correct to say, as the displacement or momentum thickness increases, since these parameters are more appropriate measures of the combined effects of boundary layer thickness and the shape of

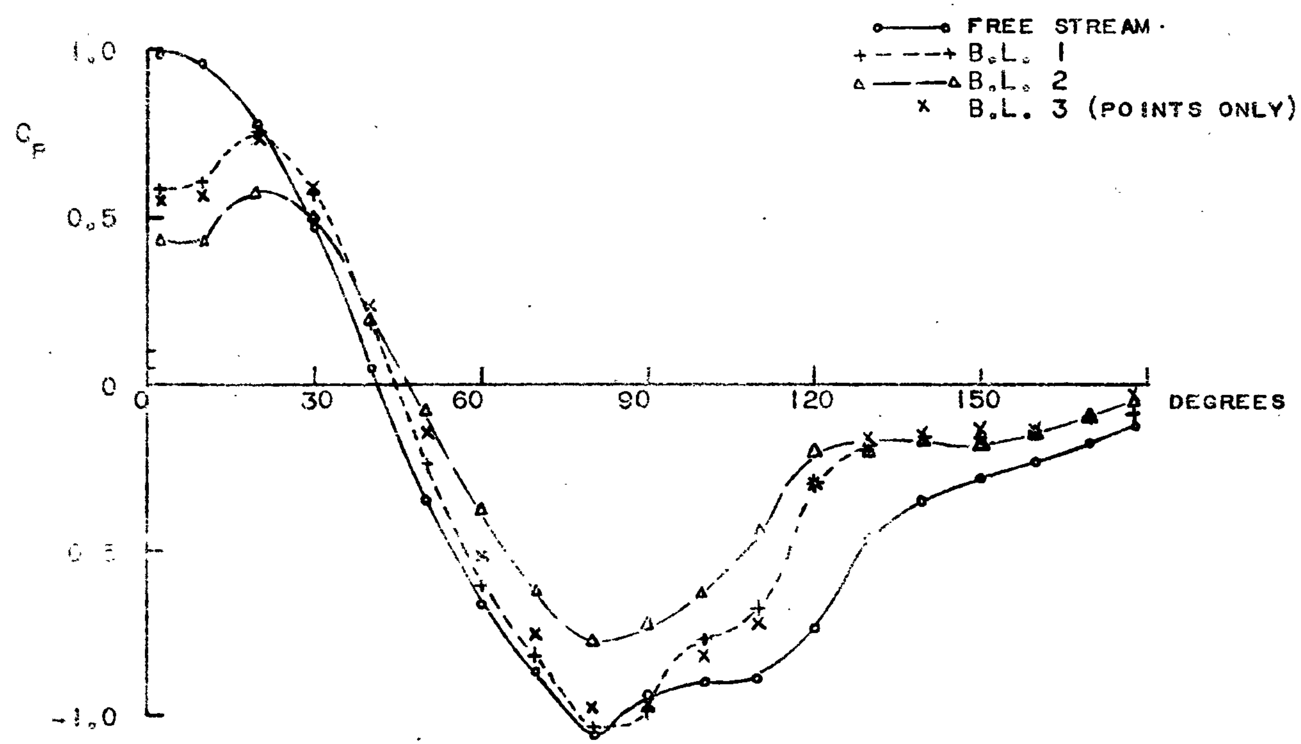

FIGURE 4 - COMPARISON OF CENTERLINE PRESSURE DISTRIBUTIONS FOR A 4.25 INCH DIAMETER SPHERE

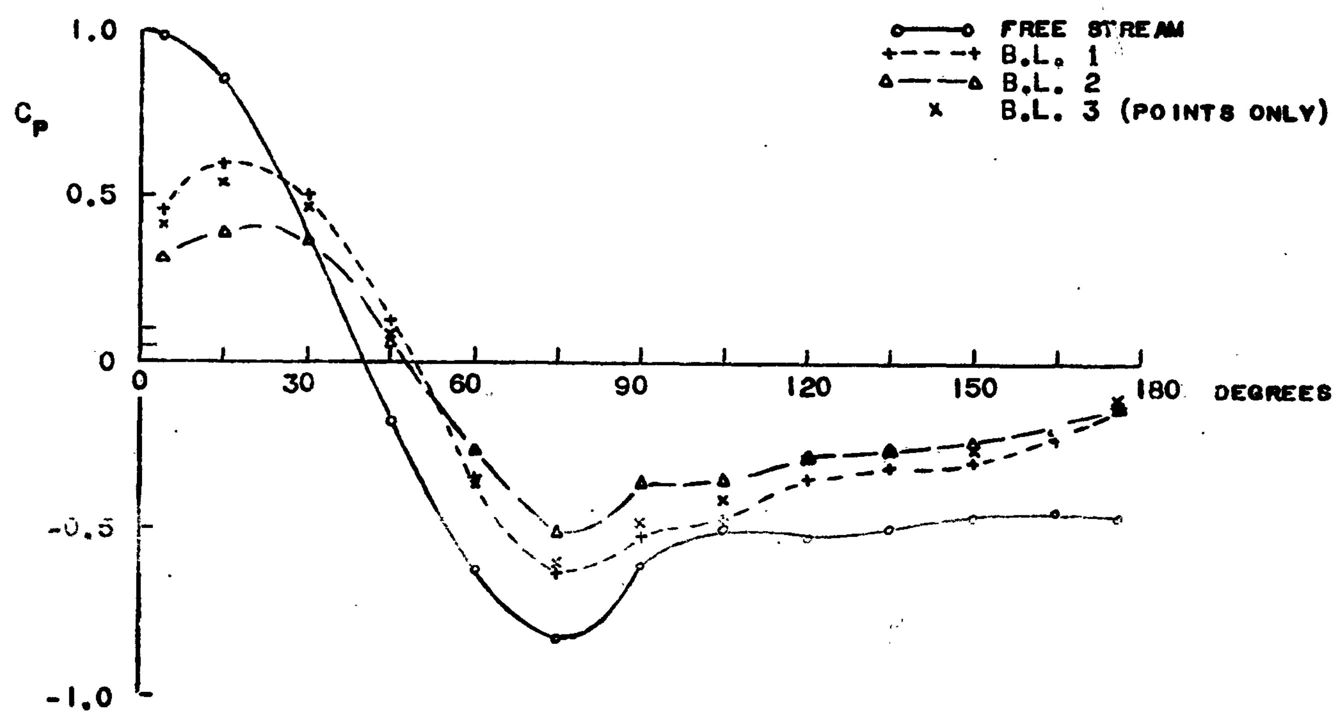

FIGURE 5 - COMPARISON OF CENTERLINE PRESSURE DISTRIBUTIONS FOR 2.22 INCH DIAMETER SPHERE

the velocity profile. Hence, increasing the thickness of the friction layer reduces the ordinates of the free-stream pressure distribution.

Figure 6 shows pressure distributions on the large and small semicylinders where the ratios δ/D and δ^*/D were approximately the same. One would normally expect these results to be in closer agreement. It is believed that the additional turbulence introduced by the simulated boundary layer on the larger semicylinder stabilized the flow and enabled the flow to reach a lower negative pressure coefficient and to achieve better pressure recovery at the rear. The Reynolds numbers for the large and small cylinders were 1.6×10^5 and 0.6×10^5, respectively (based on diameter and free-stream velocity). In a uniform flow these values of Reynolds number would be in the range near transition for a cylinder (Reference 6, Figure 152), similar to the case of the spheres already discussed. The differences in the two pressure distributions on the semicylinders are believed to be analagous to the effects of free-stream turbulence and Reynolds number already discussed in connection with the two hemispherical models. Pressure distributions for the other boundary layer conditions on the semicylinders are shown in Figures 19 and 20.

Results for the small half-model are given in Figures 7 and 21 through 23. The curves in these plots are faired with emphasis on the points for the centerline pressure taps (i.e., 90° away from the wall). Figure 21 shows the free-stream pressure distribution. A similar pressure distribution previously measured in a smaller wind tunnel at a velocity of 33 feet per second is shown for comparison. Figure 7 shows a crossplot for all of the conditions tested. It can be seen that the effect of increasing boundary layer thickness is the same as for the hemisphere and semicylinder models (i.e., the positive and negative pressures become smaller as the boundary layer thickness increases). Figures 22 and 23 show the pressures for the separate boundary layer conditions.

There appears to be a tendency for the pressures next to the wall to be slightly lower than the centerline pressures. The consistency of this effect is obscured by the scatter of the data and the fact that the differences are about the same order of magnitude as the precision of the measurements. Disregarding this small effect, one could say that the pressures at a given longitudinal location are approximately the same. A similar approximation can be made for the hemispherical models by recording the pressures on a true plan view and fairing in contours of equal pressures.

Results for the large half-model are shown in Figures 8 and 24 through 26. These measurements show essentially the same characteristics as those already discussed for the preceding cases.

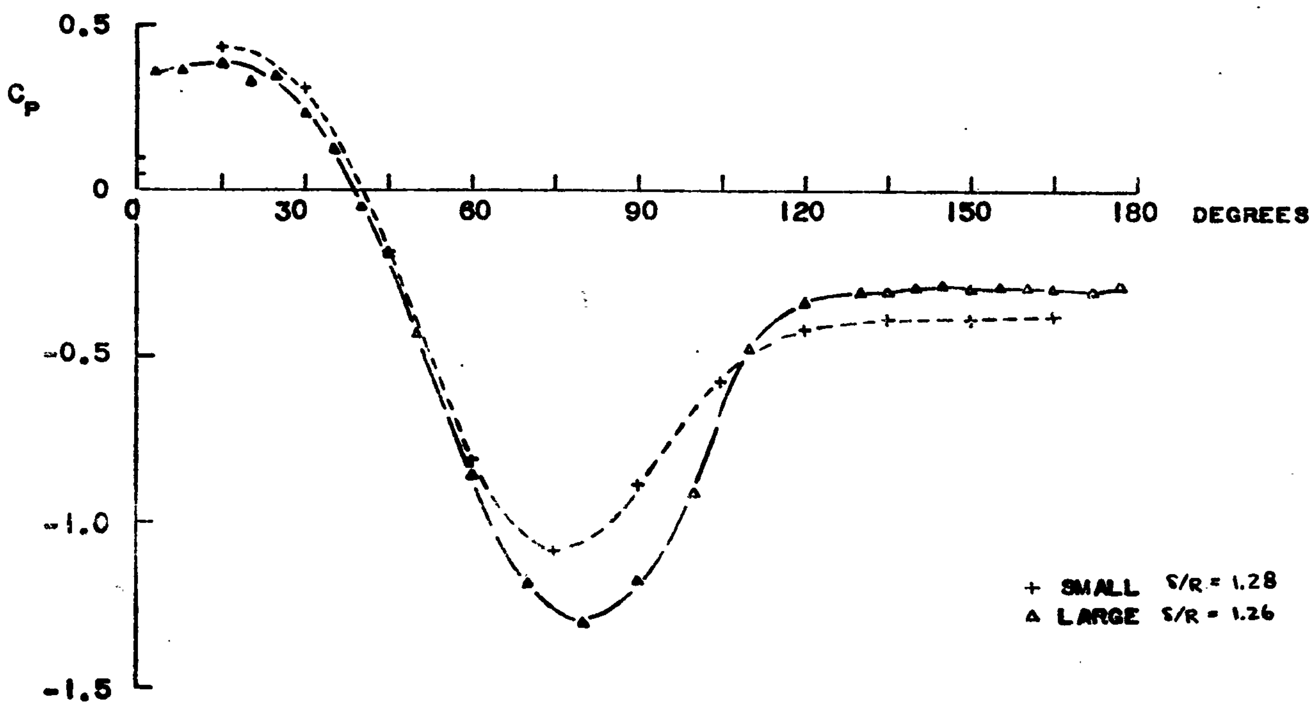

FIGURE 6 - COMPARISON OF PRESSURE DISTRIBUTIONS ON TWO SEMICYLINDERS

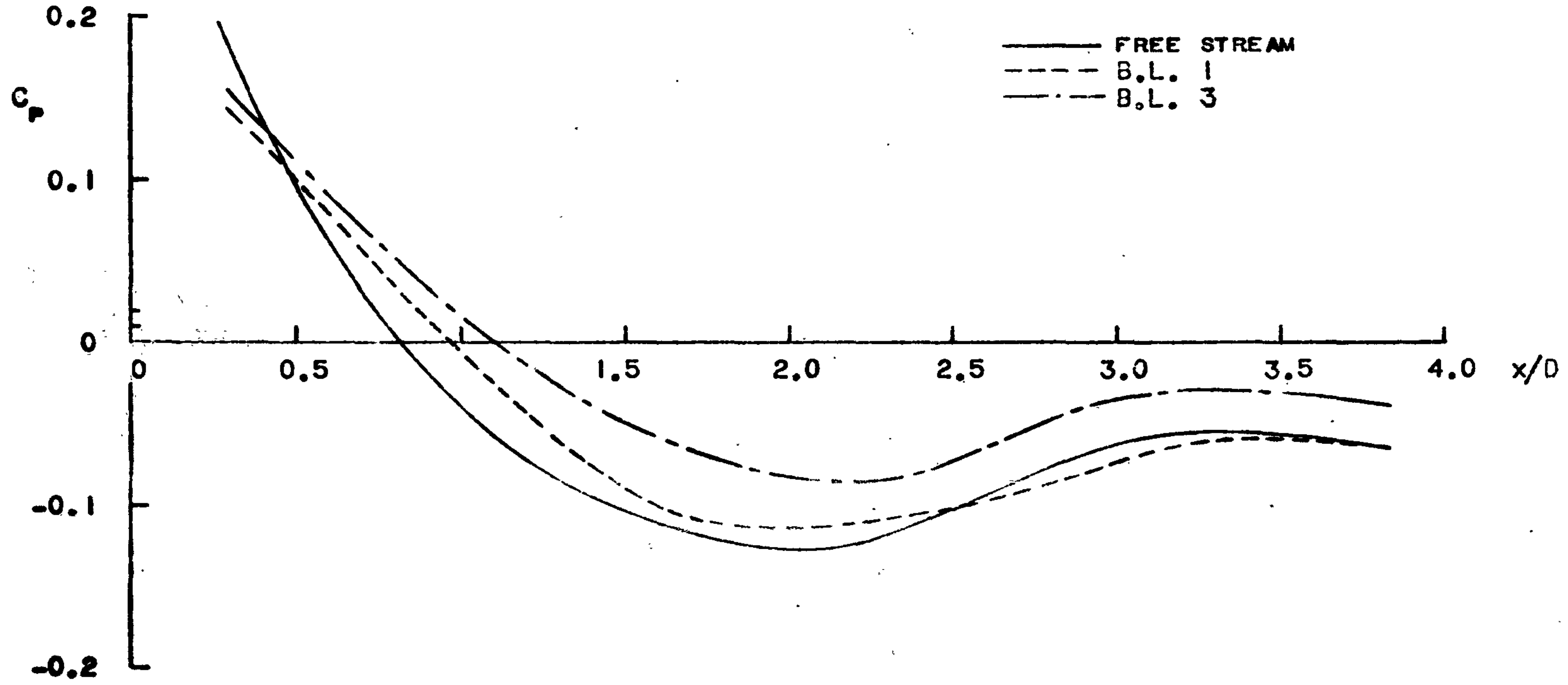

FIGURE 7 - PRESSURE DISTRIBUTIONS ON SMALL HALF-MODEL

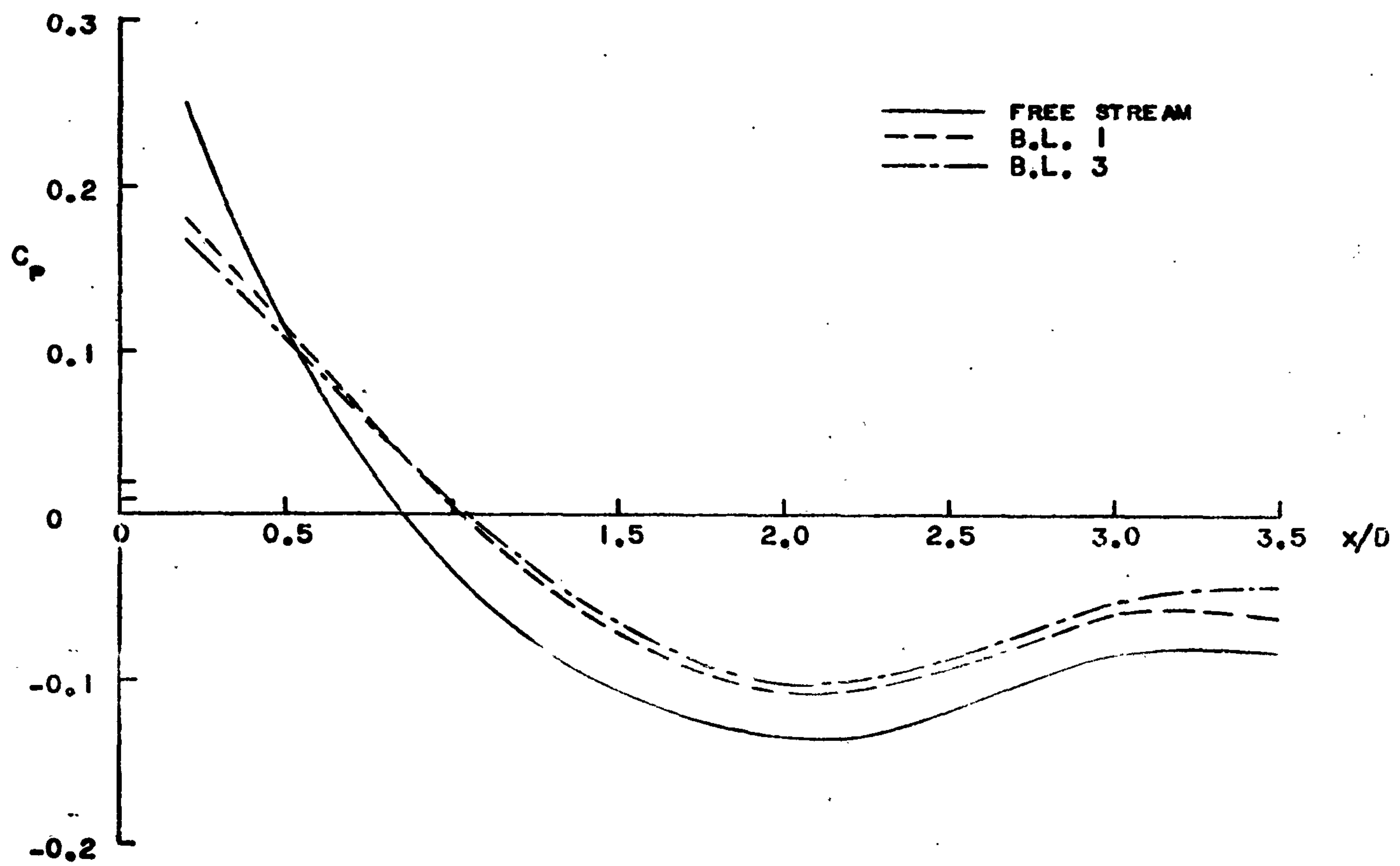

FIGURE 8 - PRESSURE DISTRIBUTIONS ON LARGE HALF-MODEL

One of the objectives of the present series of tests was to obtain results which would improve the understanding of pressure distributions in a flow with a velocity gradient. The qualitative similarities in the present results for both the two- and three-dimensional models has already been discussed. A more useful corollary would be to obtain a quantitative method for modifying a pressure distribution measured under one set of conditions to estimate what that pressure distribution would be like under different boundary layer conditions. One might attempt to redefine the pressure coefficient since increasing the boundary layer thickness reduces the ordinates of the pressure distribution plot. However, it can be seen that a simple redefinition (such as using a different characteristic velocity or dynamic pressure) would not work since the ordinates are not reduced uniformly over the length of the body. This can be seen from the shape of the pressure distribution near the stagnation points of the hemispheres and semicylinders and the shift in the locations of zero pressure coefficient for all cases. Although a general transformation was not found, it was noted that plots of C_{pmin} versus δ^* or θ were approximately linear and had (about) the same slope for all models. Figure 9 shows a plot which combines results from all models. Points for the semicylinders were included by estimating a C_{pmin} for the free stream condition by extrapolating C_p to $\theta = 0$ on a plot of C_{pmin} versus θ. Table 3 summarizes values used in Figure 9 and other characteristics for various model-boundary layer conditions.

SUMMARY

Pressure distributions were measured on six models in three different boundary layer conditions. The effect of increasing boundary layer thickness (or momentum thickness) was a reduction in the positive and negative ordinates of the free-stream pressure distribution. The pressures on three-dimensional models were approximately the same at a given longitudinal station, although there may have been a small reduction in pressures close to the wall on which the object was mounted. A data correlation was obtained relating C_{pmin} for a given boundary layer condition and C_{pmin} measured in a uniform flow.

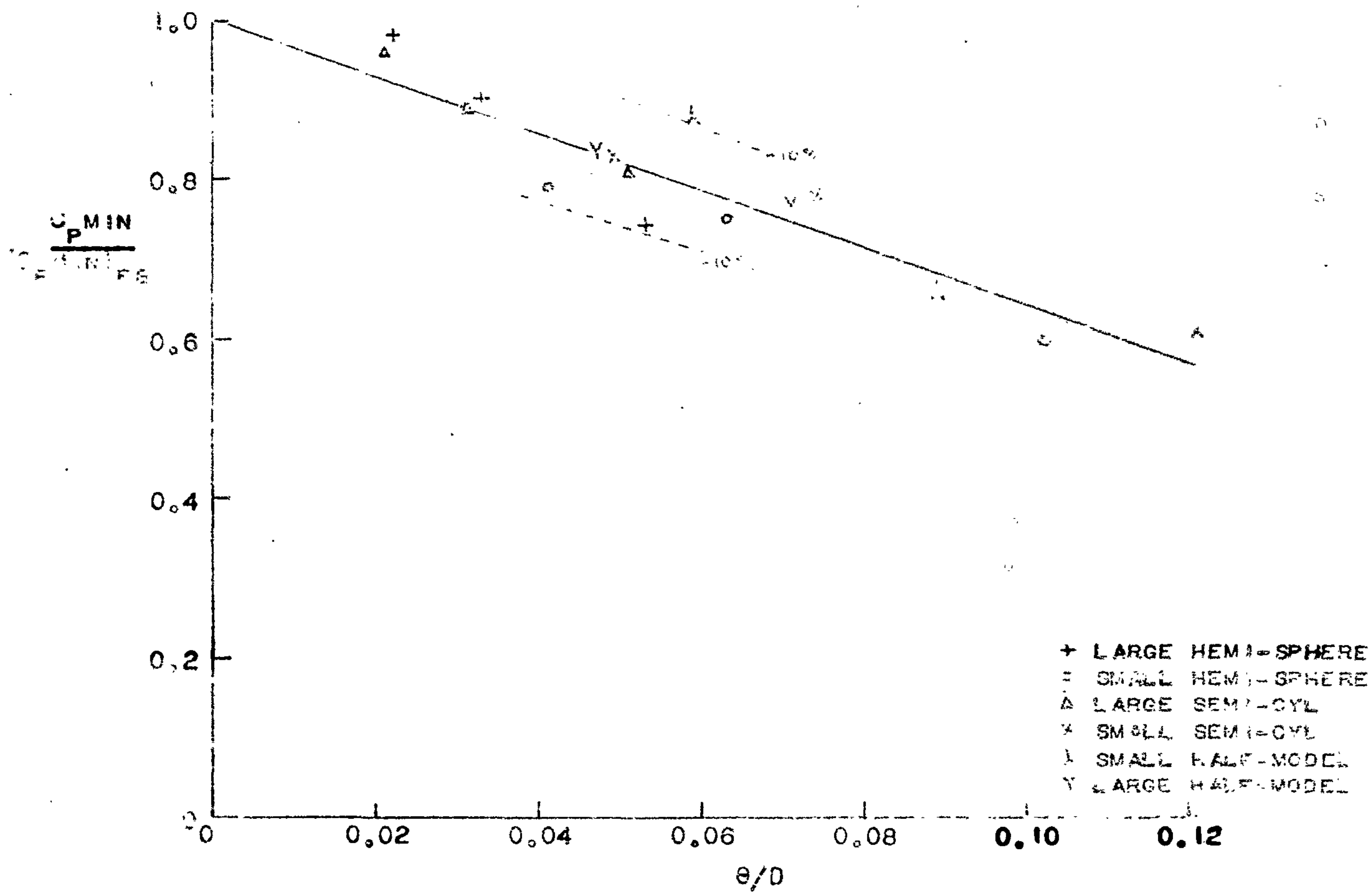

FIGURE 9 - DATA CORRELATION FOR MINIMUM PRESSURE COEFFICIENT

TABLE 1 - Offsets for Half-models

Small Half-model

x/D_m	0.28	0.42	0.65	1.12	1.60	2.10	2.59	3.22	3.83
D - in	0.41	0.55	0.78	1.10	1.36	1.51	1.57	1.57	1.57

Large Half-model

x/D_m	0.20	0.64	1.11	1.58	2.06	2.54	3.03	3.48
D - in	0.32	0.90	1.33	1.68	1.89	1.96	1.96	1.96

TABLE 2 - Boundary Layer Properties

BL	δ in	δ^* in	θ in	δ^*/δ	θ/δ^*	θ/δ
1	1.2	0.121	0.092	0.099	0.760	0.0767
2	2.8	0.308	0.227	0.110	0.738	0.0810
3	2.4	0.186	0 139	0.0775	0.748	0.0580

TABLE 3 - Miscellaneous Model-Boundary Layer Characteristics

model	BL	$C_{p\min}$	δ^*/D	θ/D	$\frac{C_{p\min}}{C_{p\min}(F.S.)}$
small sphere (D = 2.22")	FS	-0.85	0	0	1.0
	1	-0.67	0.054	0.041	0.79
	2	-0.51	0.139	0.102	0.60
	3	-0.64	0.084	0.063	0.75
large sphere (D = 4.25")	FS	-1.05	0	0	1.0
	1	-1.03	0.028	0.022	0.98
	2	-0.78	0.072	0.053	0.74
	3	-0.94	0.044	0.033	0.90
small cyl. (D = 1.88")	FS	-1.32#	0	0	1.0
	1	-1.10	0.064	0.049	0.83
	2	-0.80	0.164	0.121	0.61
	3	-1.03	0.099	0.074	0.78

estimated

TABLE 3 - ctd.

model	BL	C_{p}min	δ^*/D	θ/D	$\frac{C_{p\,min}}{C_{p\,min}(F.S.)}$
large cyl. (D = 4.43")	FS	-1.60#	0	0	1.0
	1	-1.54	0.027	0.021	0.96
	2	-1.30	0.070	0.051	0.81
	3	-1.42	0.042	0.031	0.89
small half-m (D = 1.57")	FS	-0.128	0	0	1.0
	1	-0.112	0.077	0.059	0.88
	3	-0.085	0.118	0.089	0.66
large half-m (D = 1.96")	FS	-0.138	0	0	1.0
	1	-0.114	0.062	0.047	0.84
	3	-0.106	0.095	0.071	0.77

estimated

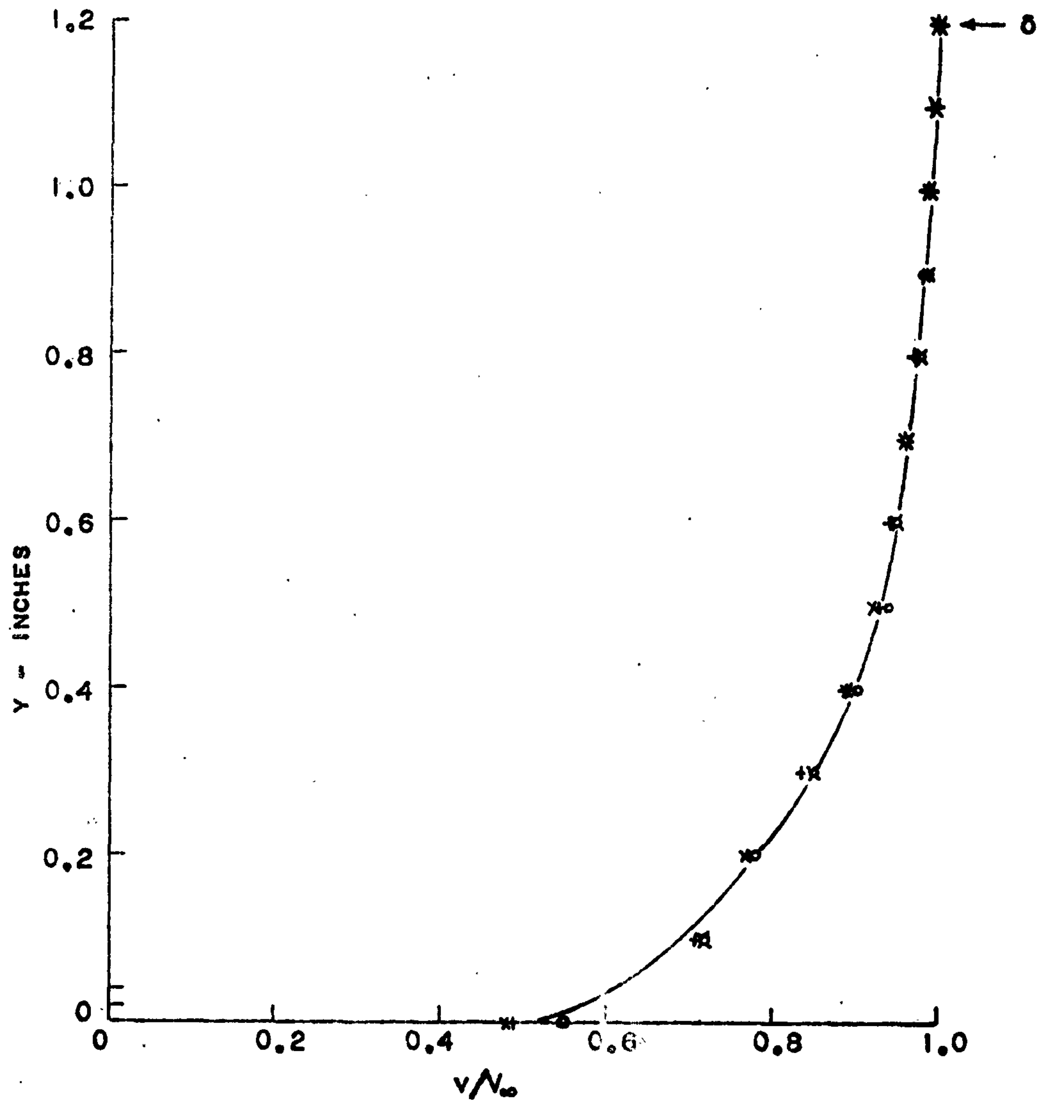

FIGURE 10 - VELOCITY PROFILE - BOUNDARY LAYER 1

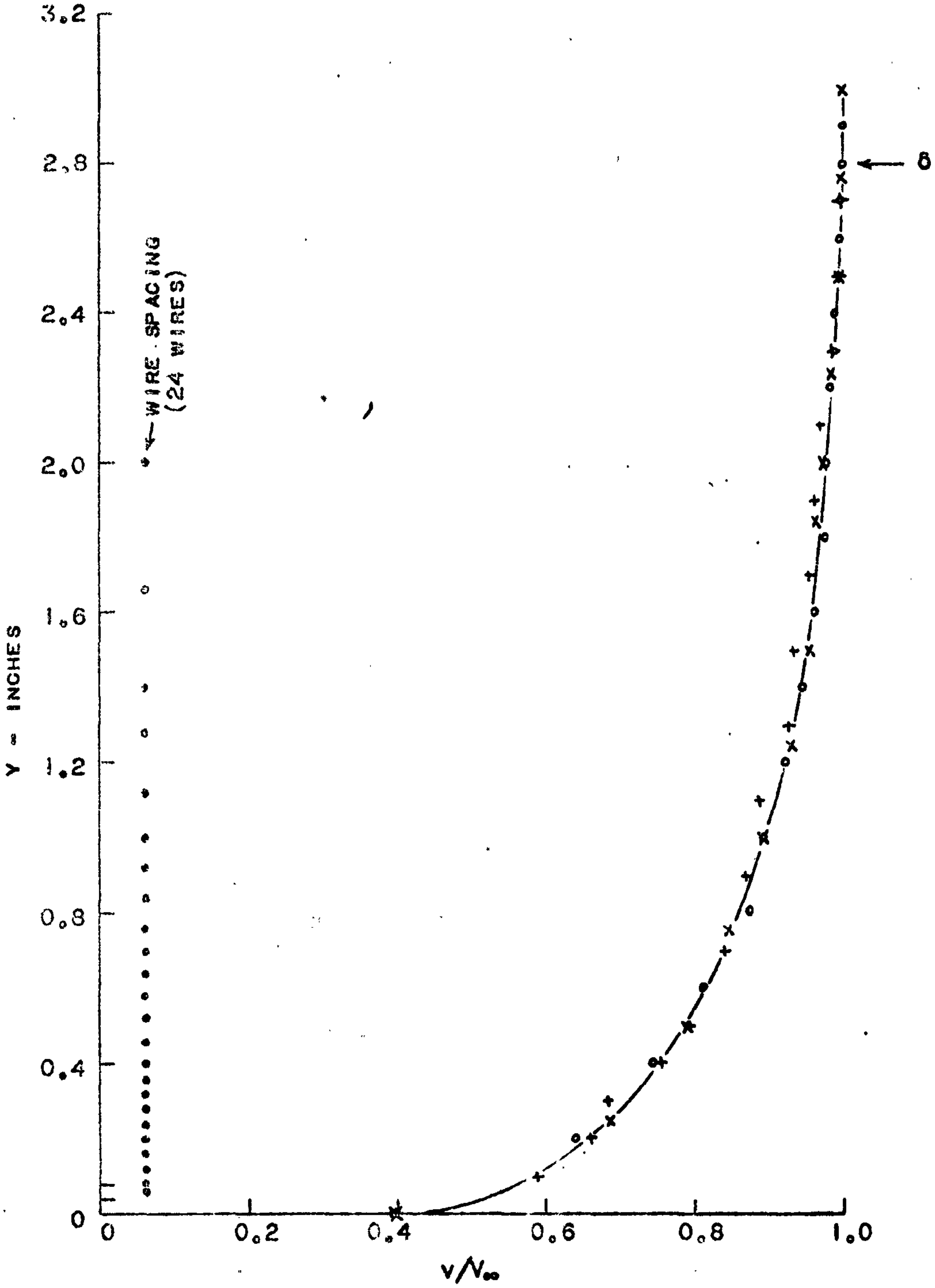

FIGURE 11 - VELOCITY PROFILE - BOUNDARY LAYER 2

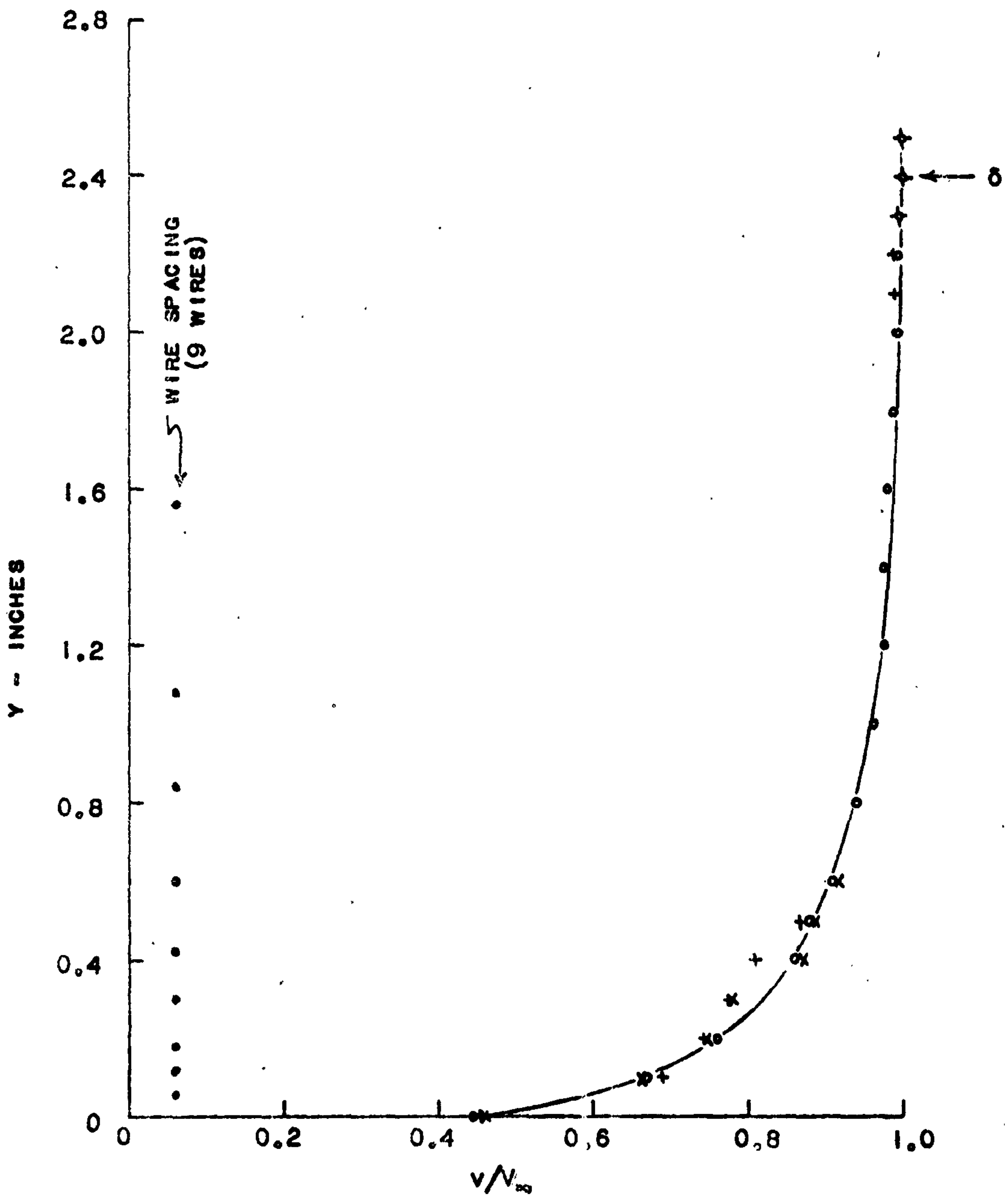

FIGURE 12 - VELOCITY PROFILE - BOUNDARY LAYER 3

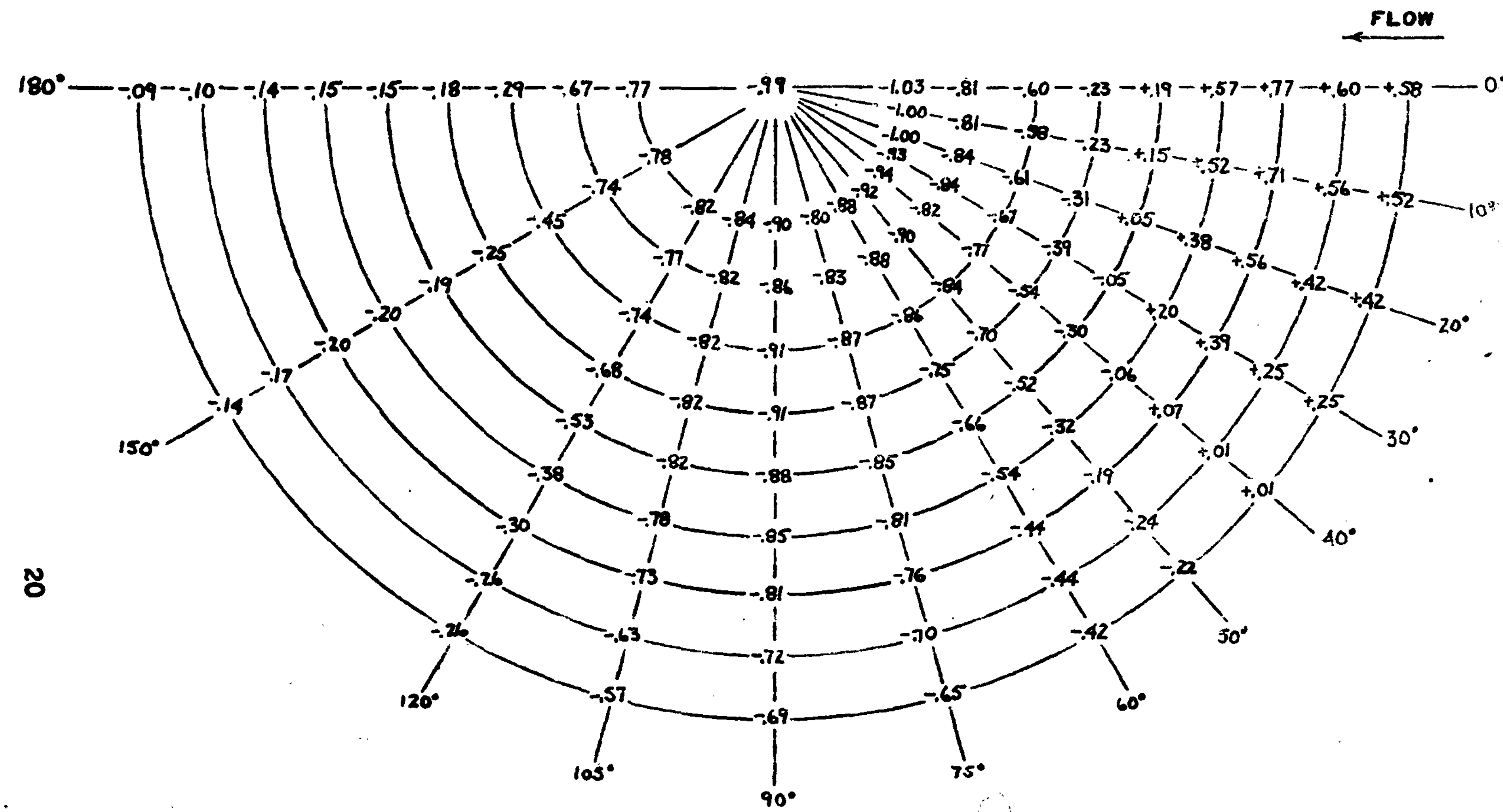

FIGURE 13 - PRESSURE PLOT - LARGE HEMISPHERE, BOUNDARY LAYER 1

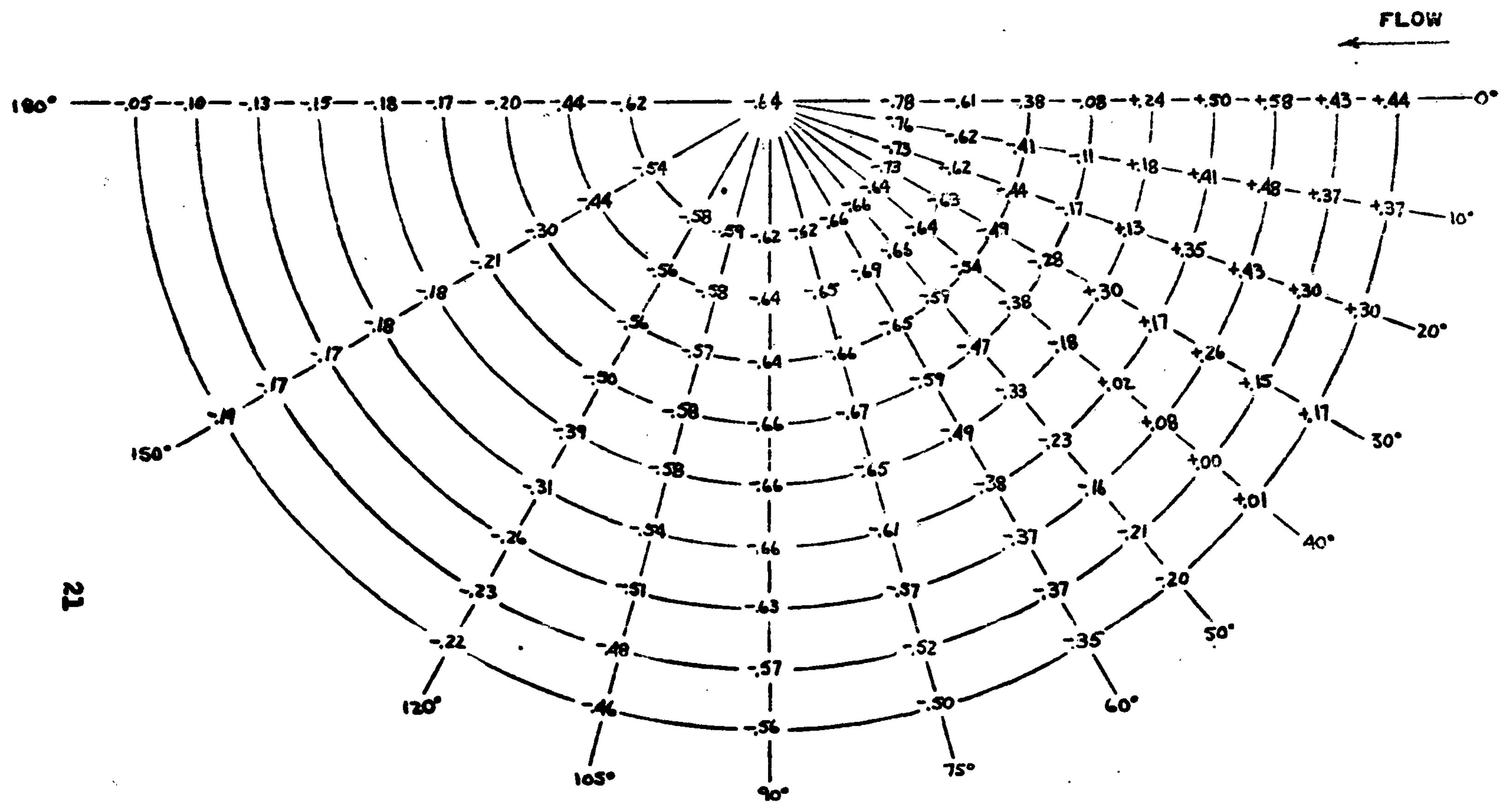

FIGURE 14 - PRESSURE PLOT - LARGE HEMISPHERE, BOUNDARY LAYER 2

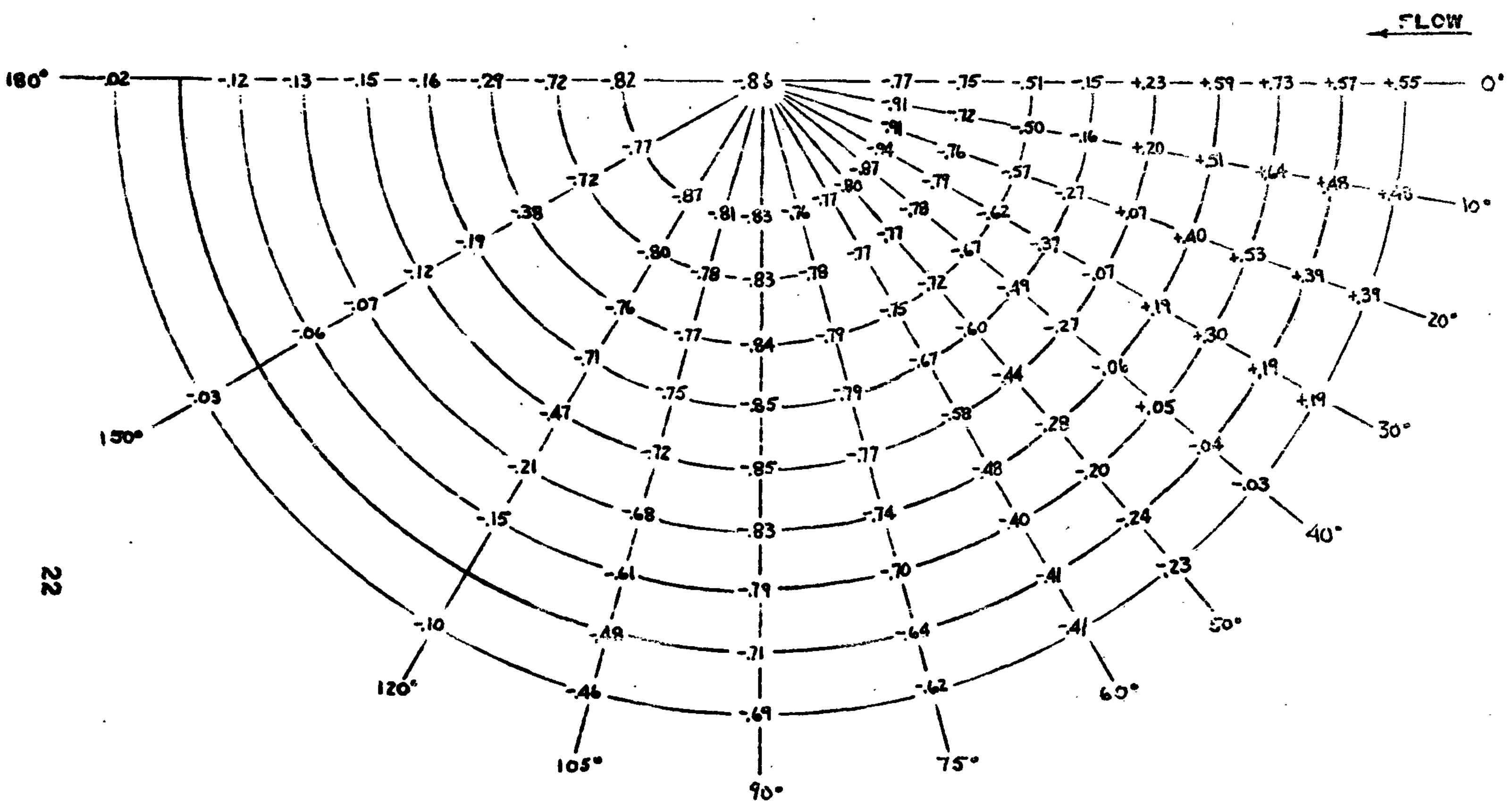

FIGURE 15 - PRESSURE PLOT - LARGE HEMISPHERE, BOUNDARY LAYER 3

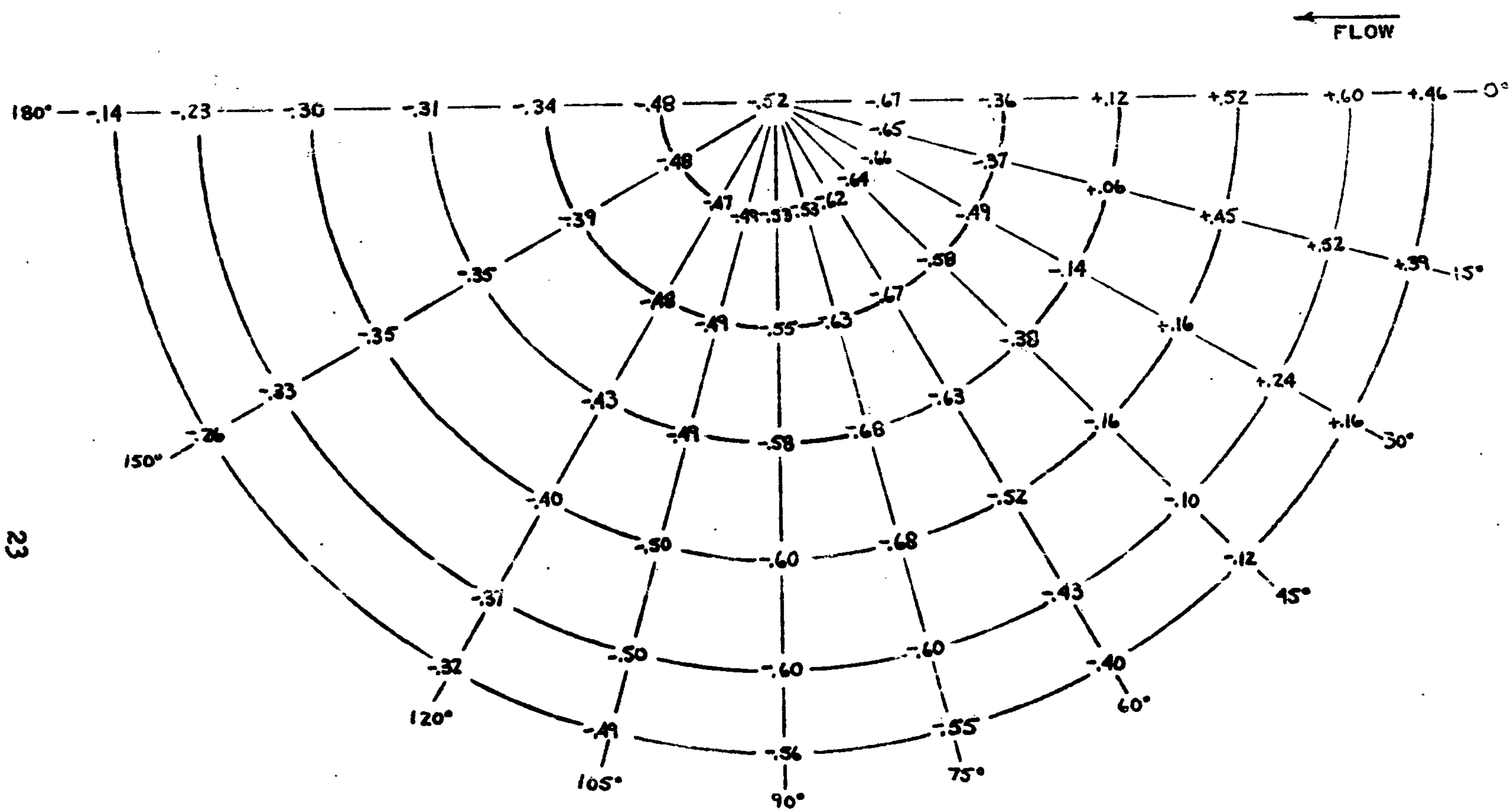

FIGURE 16 - PRESSURE PLOT - SMALL HEMISPHERE, BOUNDARY LAYER 1

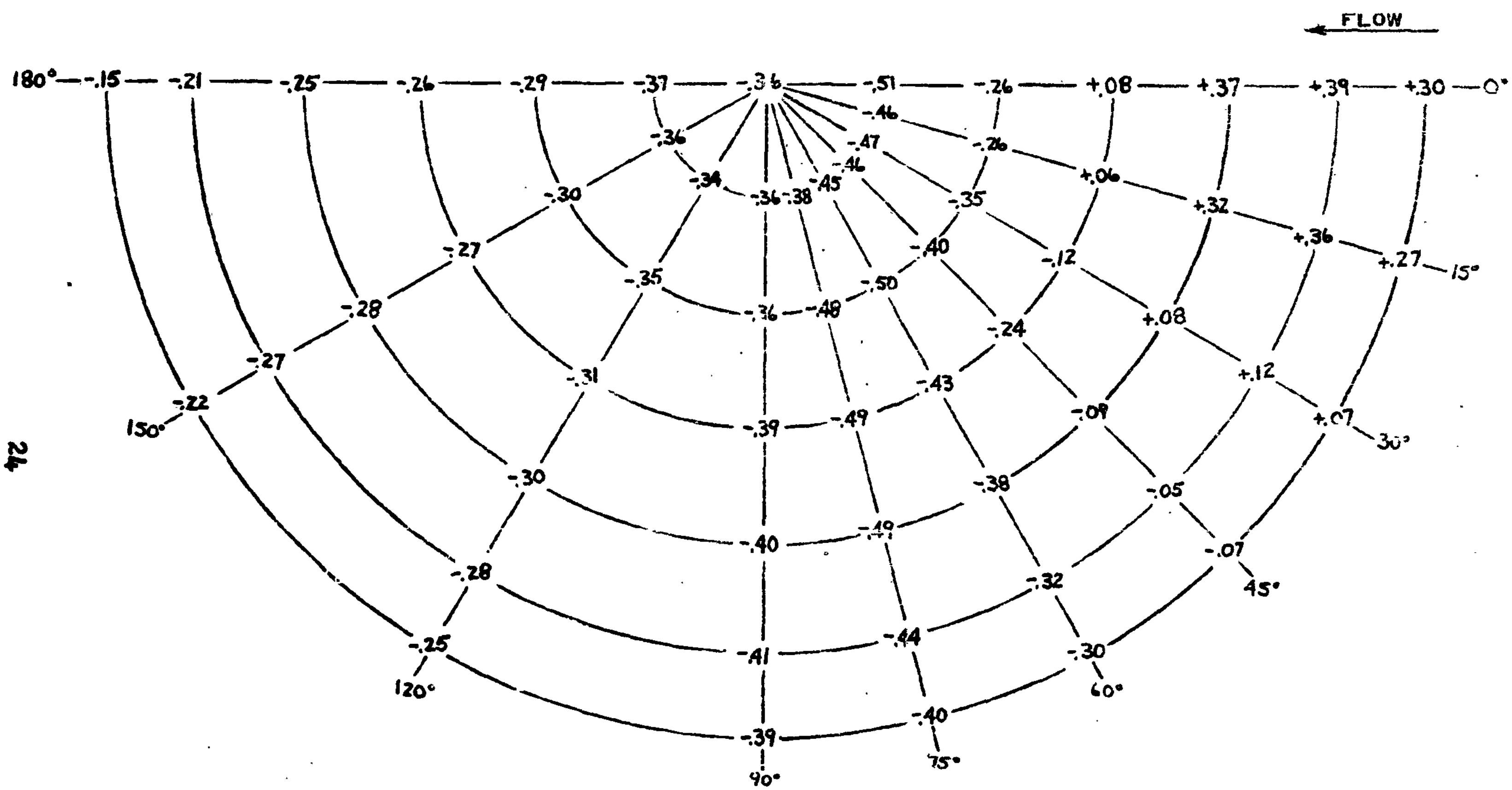

FIGURE 17 - PRESSURE PLOT - SMALL HEMISPHERE, BOUNDARY LAYER 2

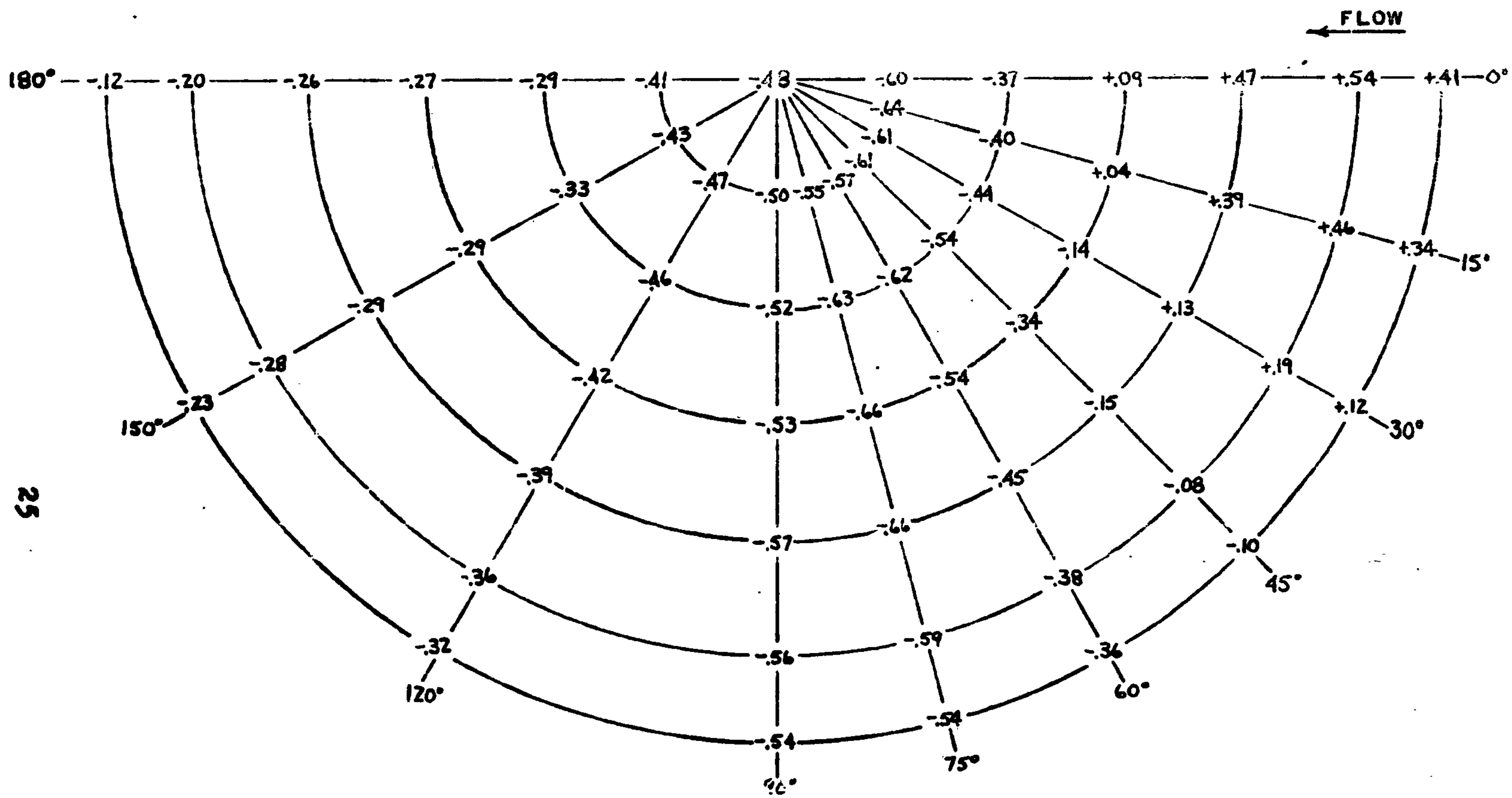

FIGURE 18 - PRESSURE PLOT - SMALL HEMISPHERE, BOUNDARY LAYER 3

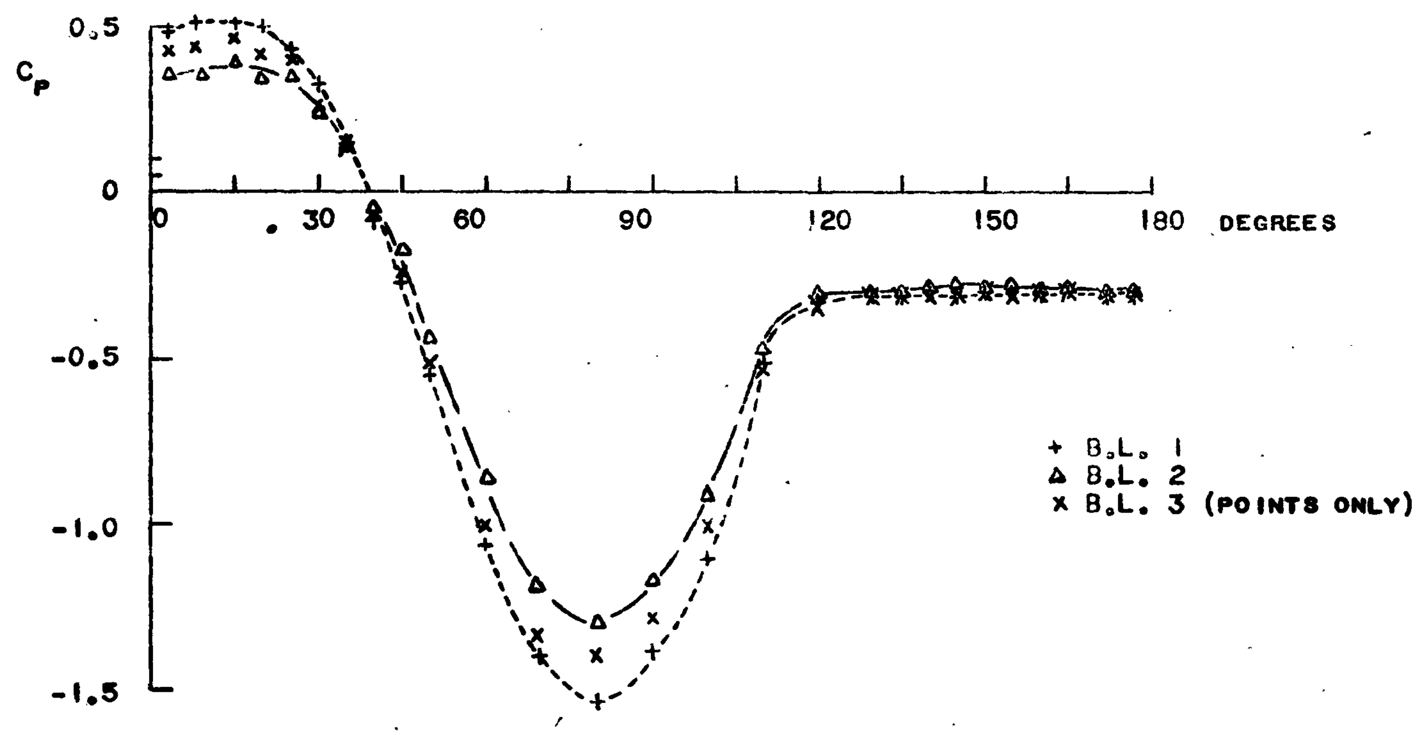

FIGURE 19 - PRESSURE DISTRIBUTIONS ON LARGE SEMICYLINDER

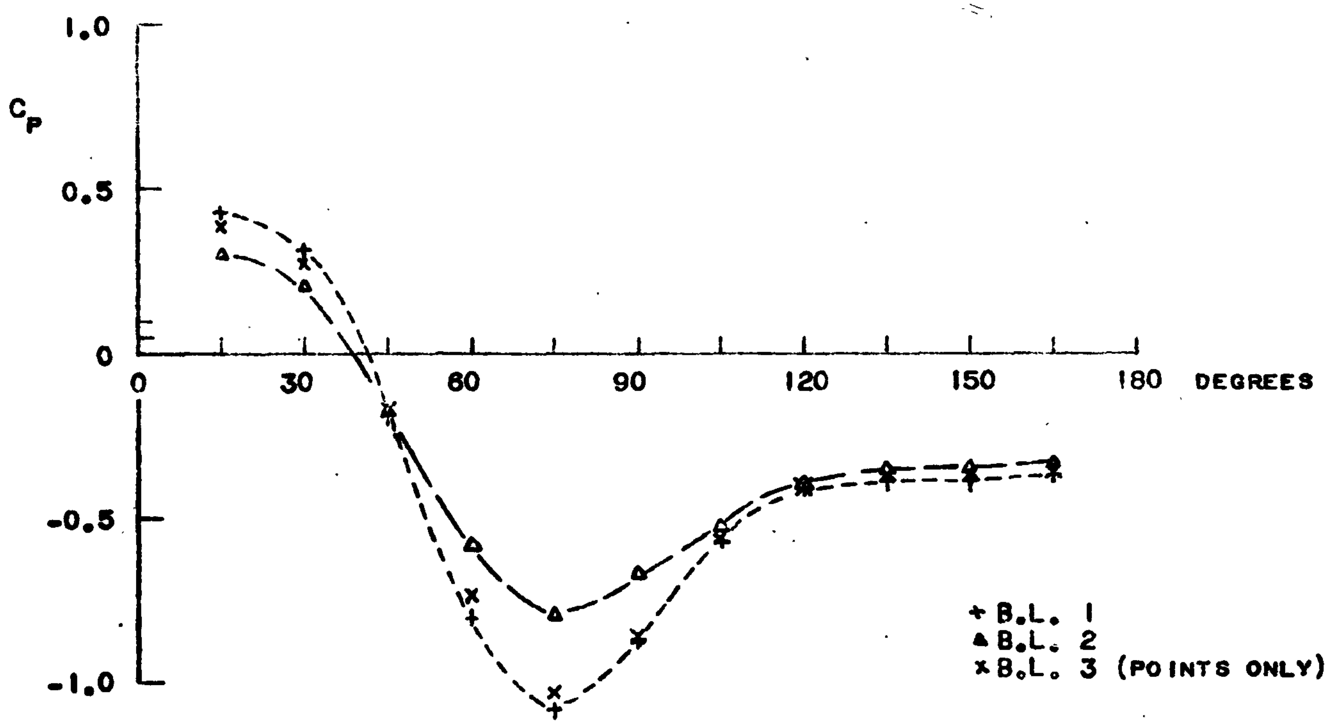

FIGURE 20 - PRESSURE DISTRIBUTIONS ON SMALL SEMICYLINDER

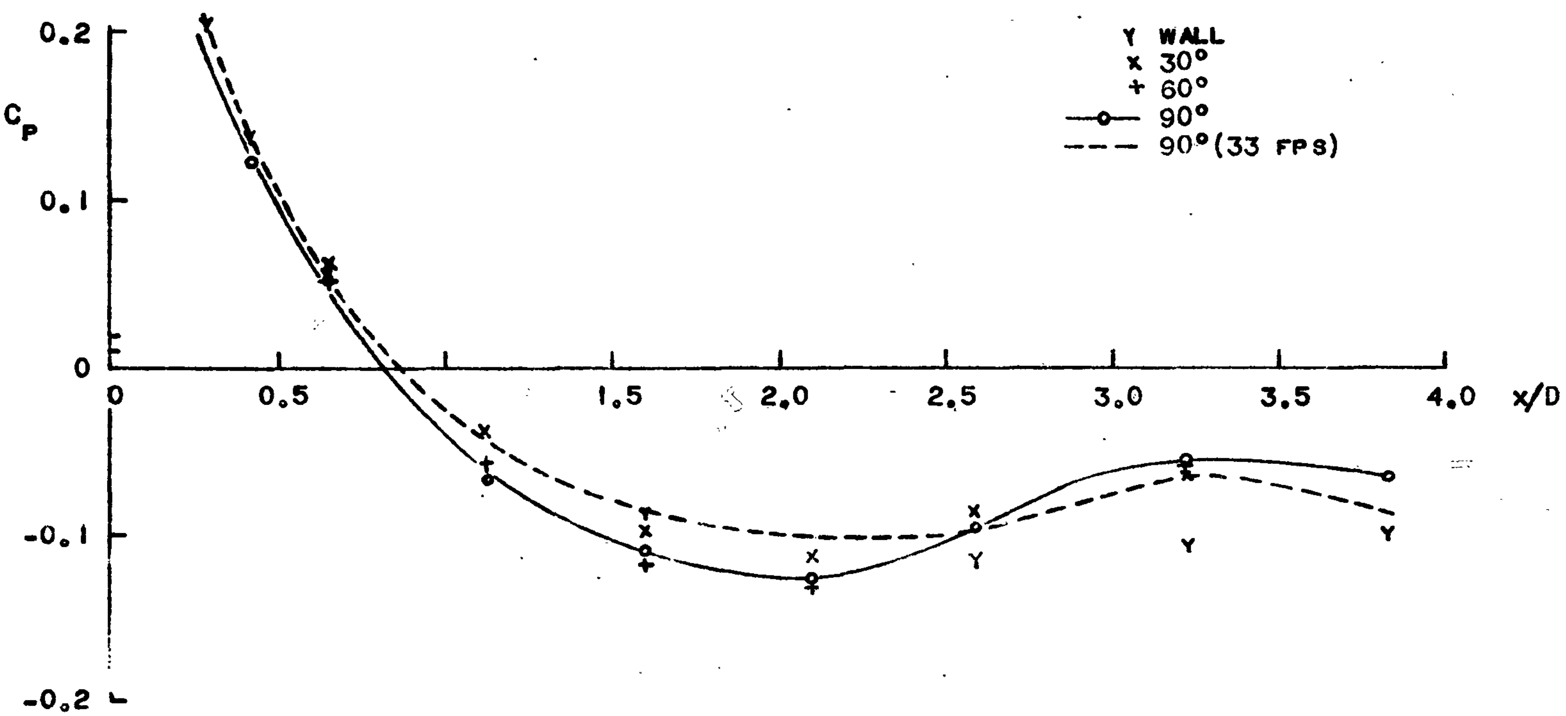

FIGURE 21 - PRESSURE DISTRIBUTIONS ON SMALL HALF-MODEL, FREE STREAM

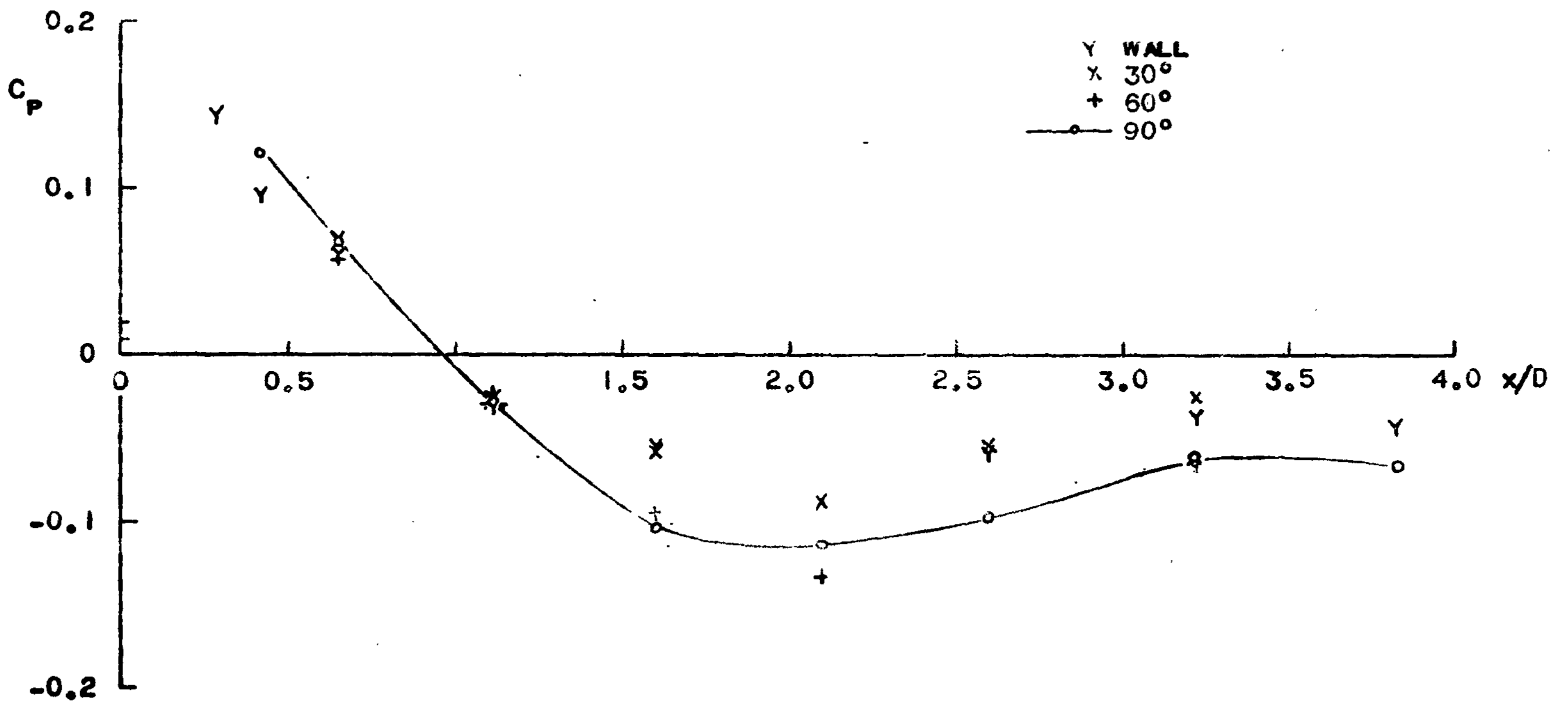

FIGURE 22 - PRESSURE DISTRIBUTIONS ON SMALL HALF-MODEL, BOUNDARY LAYER I

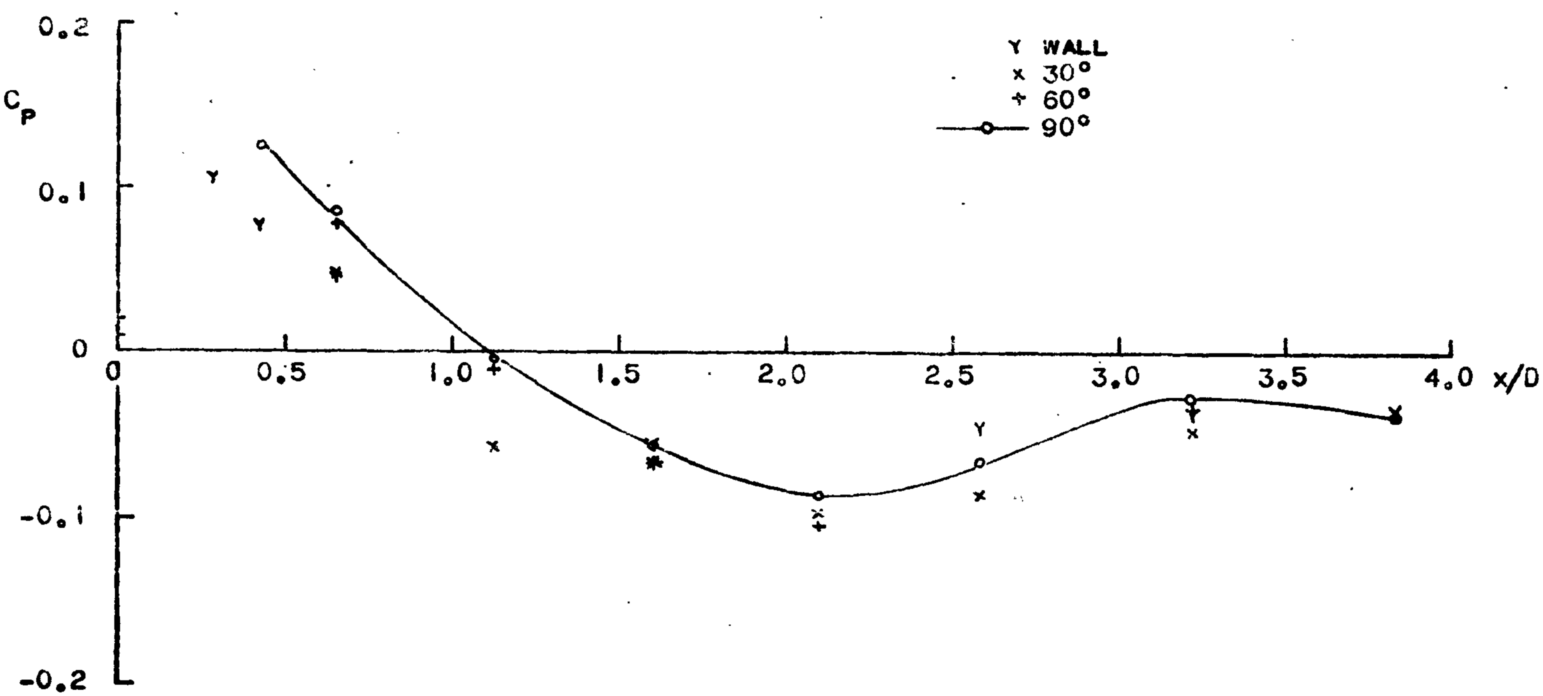

FIGURE 23 - PRESSURE DISTRIBUTIONS ON SMALL HALF-MODEL, BOUNDARY LAYER 3

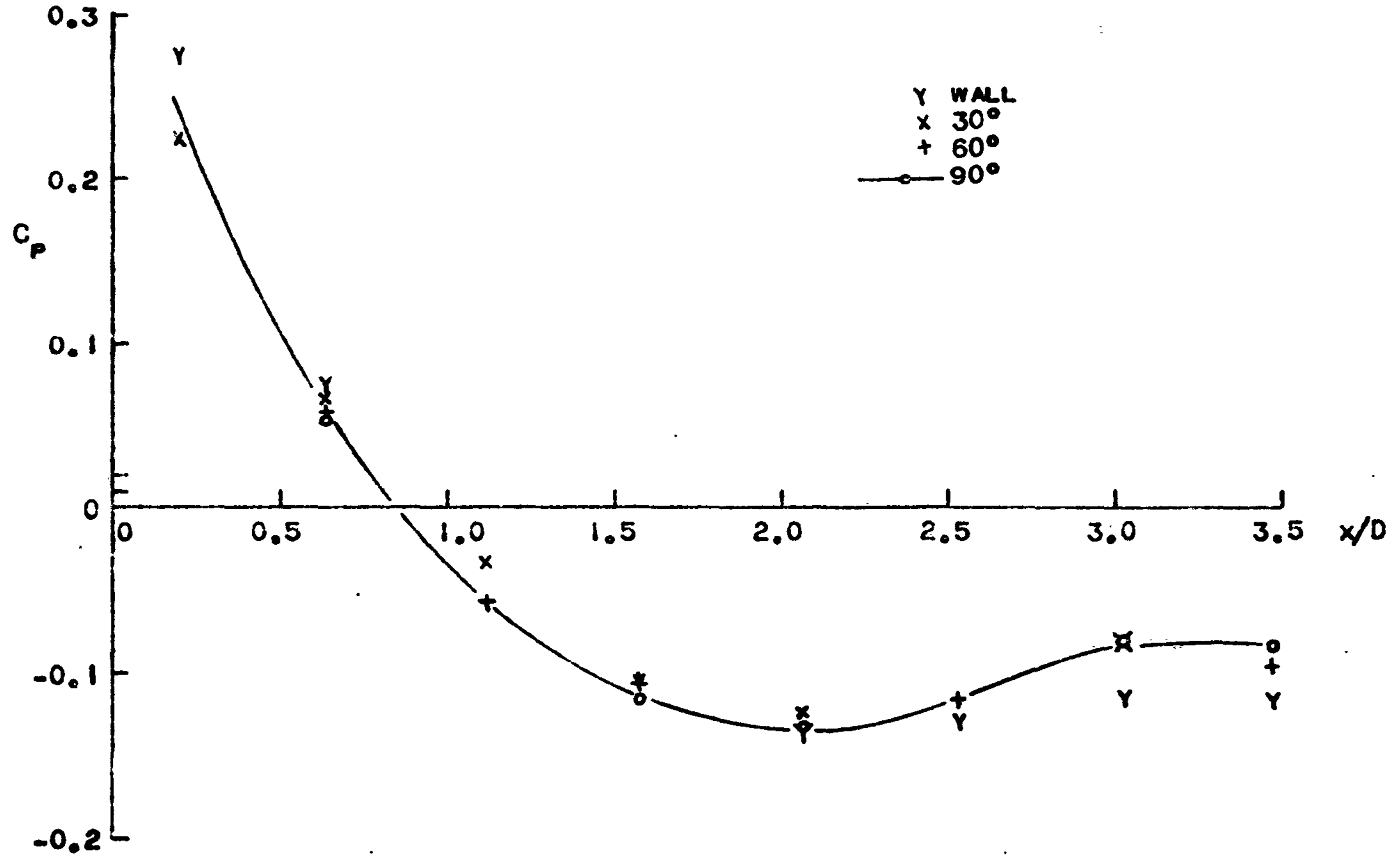

FIGURE 24 - PRESSURE DISTRIBUTIONS ON LARGE HALF-MODEL, FREE STREAM

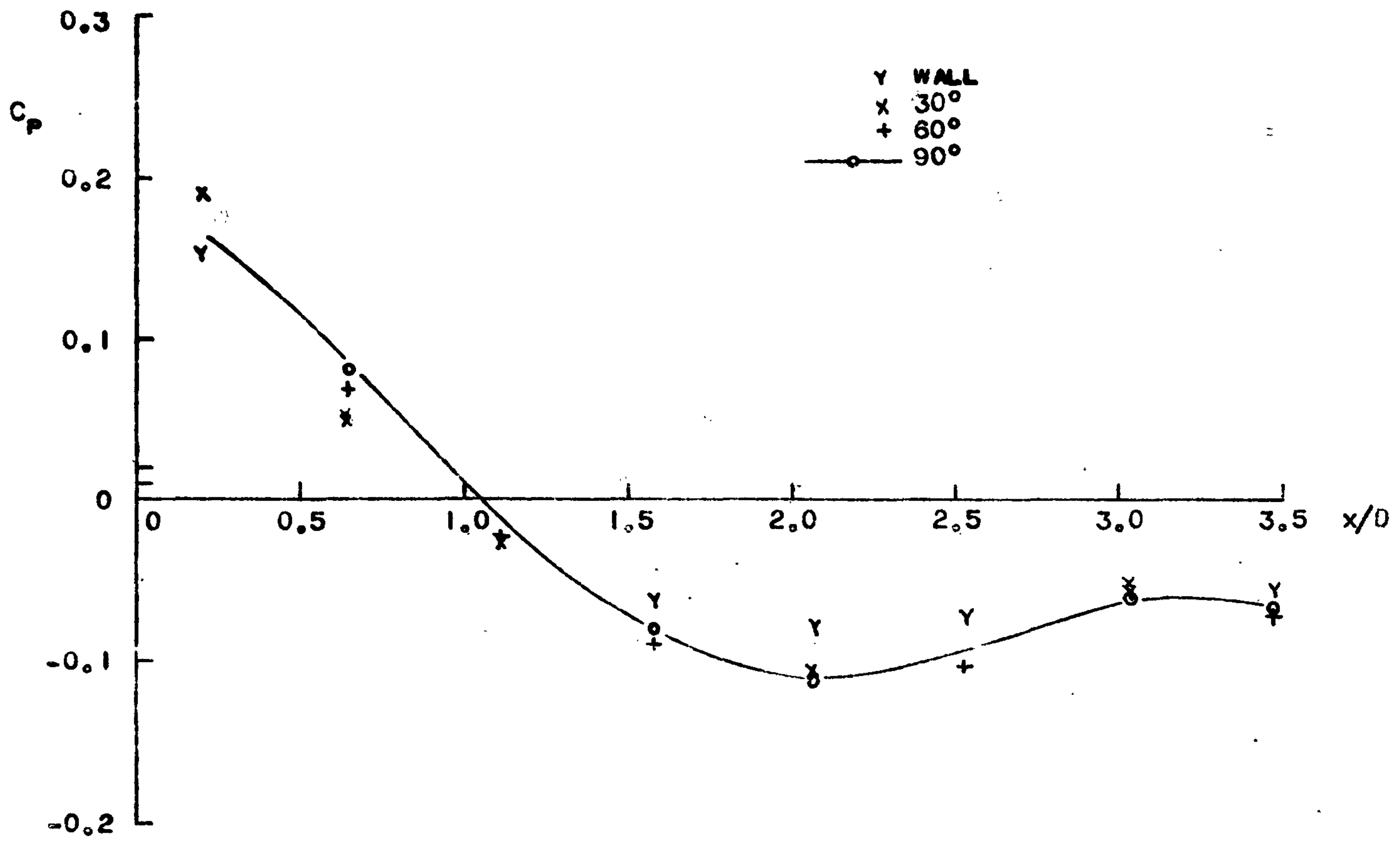

FIGURE 25 - PRESSURE DISTRIBUTIONS ON LARGE HALF-MODEL, BOUNDARY LAYER 1

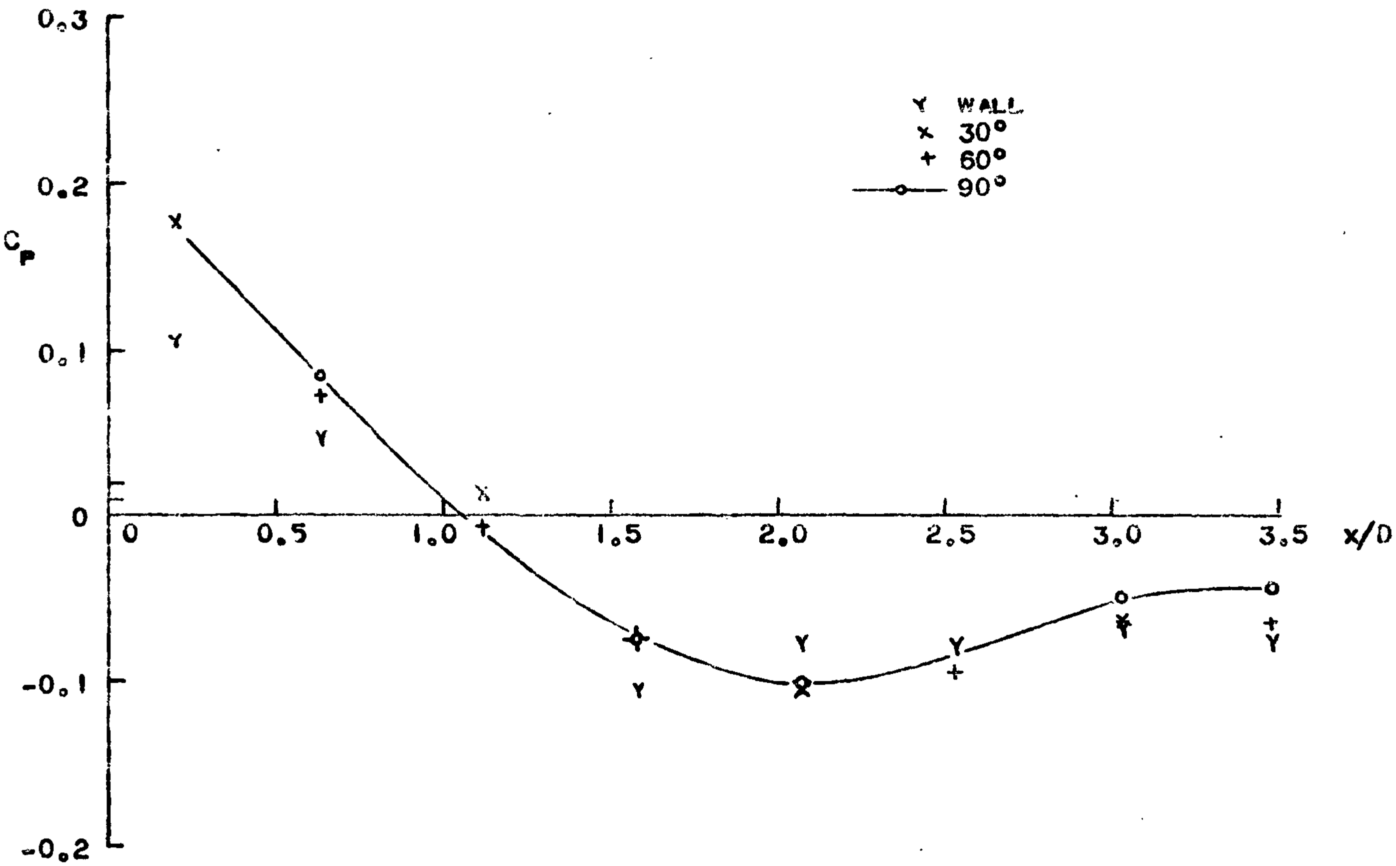

FIGURE 26 - PRESSURE DISTRIBUTIONS ON LARGE HALF-MODEL, BOUNDARY LAYER 3

ACKNOWLEDGMENTS

The present investigation was conducted under the sponsorship of ONR contract Nonr 595(19) as part of the Fundamental Hydromechanics Program of the Navy Department Bureau of Ships and administered by the Taylor Model Basin. The author appreciates the assistance of Mr. Frank Buckley in calibrating the wind tunnel, developing the technique for the construction of the hemisphere models, and devising a method for producing the artificial boundary layers. Mr. Douglas Dockery provided valuable assistance in conducting the tests and reducing the wind tunnel data.

LIST of REFERENCES

1. Weighardt, K., "Increase of Turbulent Frictional Resistance Caused by Surface Irregularities," Jahrbuch der deutschen Luftfahrt forschung (1943).

2. Tillman, W., "Additional Measurements of the Drag of Surface Irregularities in Turbulent Boundary Layers," NACA TM 1299 (1951).

3. Jobin W. and Ippen, A., "Ecological Design of Irrigation Canals for Snail Control," Science, Vol. 145, p. 1324, (Sept. 18, 1964).

4. Holl, J. W., "The Inception of Cavitation on Isolated Surface Irregularities," Transactions of the ASME, Journal of Basic Engineering, Vol. 82, no. 1, p. 169, (March 1960).

5. Schlichting, H., "Boundary Layer Theory," first ed. Pergamon Press, N.Y., Chapter 21 (1955).

6. Goldstein, S., "Modern Developments in Fluid Dynamics," Oxford Press, Vol. 2 (1938).

INITIAL DISTRIBUTION LIST

7 Chief, Bureau of Ships
Department of the Navy
Washington 25, D.C.
Code 341B (1) Code 421 (1)
Code 345 (1) Code 436 (1)
Code 420 (1) Code 210L (1)

1 Commanding Officer
Office of Naval Research, Branch Office
485 Summer Street
Boston 10, Massachusetts

1 Commanding Officer
Office of Naval Research, Branch Office
207 West 24th Street
New York 11, New York

1 Commanding Officer
Office of Naval Research, Branch Office
219 So. Dearborn Street
Chicago 1, Illinois

1 Commanding Officer
Office of Naval Research, Branch Office
1000 Geary Street
San Francisco 9, California

1 Commanding Officer
Office of Naval Research, Branch Office
1050 East Green Street
Pasadena 1, California

2 Director
Naval Research Laboratory
Washington 25, D.C.
Attn: Code 2021

2 Commander
Naval Ordnance Laboratory
White Oak
Silver Spring, Maryland
Attn: Library

2 National Aeronautics & Space Administration
1512 H Street NW
Washington 25, D.C.

20 Defense Documentation Center
Cameron Station
Alexandria, Virginia

1 Society of Naval Architects & Marine Engineers
74 Trinity Place
New York 6, New York
Attn: Librarian

2 Office of Naval Research
Code 438
Department of the Navy
Washington 25, D.C.

75 Commanding Officer & Director
David Taylor Model Basin
Department of the Navy
Washington 7, D.C.

Attn: Code 513

1 Aeronautical Research Associates of Princeton, Inc.
50 Washington Road
Princeton, New Jersey

1 Bolt Beranek and Newman, Inc.
Attn: Dr. Francis J. Jackson
50 Moulton Street
Cambridge 38, Massachusetts

1 Cambridge Acoustical Associates, Inc.
Attn: Dr. J. V. Rattaya
129 Mount Auburn Street
Cambridge 38, Massachusetts

1 Colorado State University
Department of Civil Engineering
Attn: Prof. J.E. Cermak
Fort Collins, Colorado

1 University of Connecticut
School of Engineering
Department of Civil Engineering
Attn: Prof. Ronald S. Brand
Storrs, Connecticut

1 Massachusetts Institute of Technology
Dept. of Aeronautics & Astronautics
Attn: Prof. Holt Ashley
Cambridge 39, Massachusetts

1 Massachusetts Institute of Technology
Gas Turbine Laboratory
Attn: Mr. Hal L. Moses
Cambridge 39, Massachusetts

1 University of Minnesota
St. Anthony Falls Hydraulic Laboratory
Attn: Director
Minneapolis 14, Minnesota

2 Ordnance Research Laboratory
Pennsylvania State University
P.O. Box 30
University Park, Pennsylvania

Attn:
Dr. Wislicenus
Dr. Lumley

1 Princeton University
School of Engineering & Applied Science
Attn: Prof. George L. Mellor
Princeton, New Jersey

1 Southwest Research Institute
Department of Mechanical Sciences
Attn: Dr. H. Norman Abramson
8500 Culebra Road
San Antonio 6, Texas

1 Stanford University
School of Engineering
Department of Civil Engineering
Attn: Prof. Robert Street
Stanford California

1 Stevens Institute of Technology
Davidson Laboratory
Attn: Dr. John P. Breslin, Director
Castle Point Station
Hoboken New Jersey

1 The University of Texas
Department of Civil Engineering
Dr. Frank D. Masch
Austin 12, Texas

1 Therm Incorporated
Therm Advanced Research
Attn: Dr. S.C. Ling
Ithaca, New York

1 Technical Research Group, Inc.
Attn: Dr. Jack Kotik
Route 110
Melville, L.I., New York

1 Vidya
Attn: Dr. H. A. Sacks
1450 Page Mill Road
Palo Alto, California

1 Oceanics, Incorporated
Attn: Dr. P. Kaplan, President
Technical Industrial Park
Plainview, L.I., New York

1 Mr. G. L. Getline
General Dynamics/Convair
Mail Zone 6-106
P.O. Box 1950
San Diego 12, California

1 U.S. Navy Underwater Sound Laboratory
Attn. Mr. J.E. Barger
New London Connecticut

1 U.S. Rubber Research Center
Attn: Dr. F. Boggs
Wayne, New Jersey

1 Bowles Engineering Company
Attn: E.E. Metzger
9347 Fraser Street
Silver Spring, Maryland

1 Cornell Aeronautical Laboratory, Inc.
Applied Mechanics Department
Attn: Dr. Irving C. Statler
P.O. Box 235
Buffalo 21, New York

1 Douglas Aircraft Company, Inc.
Aircraft Division
Long Beach, California

1 Edo Corporation
Attn: Dr. P.A. Pepper
College Point 56
Long Island, New York

1 Electric Boat Division
General Dynamics Corporation
Attn: Mr. H. E. Sheets
Groton, Connecticut

2 Illinois Institute of Technology
Technology Center
Chicago 16, Illinois
Attn: Dr. A.A. Fejer
Prof. I. Michelson

1 University of Illinois
College of Engineering
Dept. of Theoretical & Applied Mechanics
Attn: Prof. J. M. Robertson
Urbana, Illinois

1 Iowa Institute of Hydraulic Research
University of Iowa
Attn: Dr. Hunter Rouse
Iowa City, Iowa

1 The John Hopkins University
Department of Mechanics
Baltimore 18, Maryland

1 Massachusetts Institute of Technology
Research Laboratory of Electronics
Attn: Dr. George C. Maling, Jr.
Cambridge 39, Massachusetts

1 Robert Taggart, Inc.
350 Arlington Blvd.
Falls Church, Virginia

2 Hydronautics, Inc.
Pindell School Road
Fulton, Maryland

Attn: Mr. Eisenberg
Mr. Tulin

Unclassified
Security Classification

DOCUMENT CONTROL DATA - R&D

(Security classification of title, body of abstract and indexing annotation must be entered when the overall report is classified)

1. ORIGINATING ACTIVITY (Corporate author)

Mechanical Engineering Department
University of Maryland
College Park, Maryland

2a. REPORT SECURITY CLASSIFICATION
Unclassified

2b. GROUP
none

3. REPORT TITLE
AN EXPERIMENTAL STUDY OF THE EFFECTS OF BOUNDARY LAYER THICKNESS AND VELOCITY PROFILE ON THE PRESSURE DISTRIBUTIONS OF OBJECTS IMMERSED IN THE BOUNDARY LAYER

4. DESCRIPTIVE NOTES (Type of report and inclusive dates)
Final report Oct. 63- Sept. 64

5. AUTHOR(S) (Last name, first name, initial)

Sayre, Clifford L. Jr.

6. REPORT DATE	7a. TOTAL NO. OF PAGES	7b. NO. OF REFS
Feb. 1965	54	6

8a. CONTRACT OR GRANT NO.	9a. ORIGINATOR'S REPORT NUMBER(S)
Nonr 595(19)	Report No. M.E. 595(19)
b. PROJECT NO.	
c.	9b. OTHER REPORT NO(S) (Any other numbers that may be assigned this report)
d.	none

10. AVAILABILITY/LIMITATION NOTICES

Qualified requesters may obtain copies of this report from DDC.

11. SUPPLEMENTARY NOTES	12. SPONSORING MILITARY ACTIVITY
none	David Taylor Model Basin Department of the Navy Washington, D.C.

13. ABSTRACT

Pressure distributions were measured on six models in three different boundary layer conditions. Two hemispheres, two semicylinders, and two half bodies of revolution were used in the tests. The range of Reynolds numbers for the hemispheres and semicylinders was from 0.6×10^5 to 1.6×10^5 (based on diameter and free stream velocity). The boundary layer thicknesses ranged from about one-half to twice the characteristic model dimension. The effect of increasing boundary layer thickness (or momentum thickness) was a reduction in the positive and negative ordinates of the pressure distribution. The pressures on three-dimensional models were approximately the same at a given longitudinal station, although there may have been a small reduction in pressures close to the wall on which the object was mounted. No simple relationship could be found for relating the changes in pressure distribution to changes in velocity profile or boundary layer thickness, howeve. a data correlation was obtained relating the minimum pressure coefficient for a particular boundary layer condition to the minimum pressure coefficient measured in a uniform flow.

DD FORM 1 JAN 64 1473

Unclassified

Unclassified
Security Classification

14. KEY WORDS	LINK A ROLE	LINK A WT	LINK B ROLE	LINK B WT	LINK C ROLE	LINK C WT
Experiment						
Pressure Distributions						
Boundary Layer						

INSTRUCTIONS

1. ORIGINATING ACTIVITY: Enter the name and address of the contractor, subcontractor, grantee, Department of Defense activity or other organization (*corporate author*) issuing the report.

2a. REPORT SECURITY CLASSIFICATION: Enter the overall security classification of the report. Indicate whether "Restricted Data" is included. Marking is to be in accordance with appropriate security regulations.

2b. GROUP: Automatic downgrading is specified in DoD Directive 5200.10 and Armed Forces Industrial Manual. Enter the group number. Also, when applicable, show that optional markings have been used for Group 3 and Group 4 as authorized.

3. REPORT TITLE: Enter the complete report title in all capital letters. Titles in all cases should be unclassified. If a meaningful title cannot be selected without classification, show title classification in all capitals in parenthesis immediately following the title.

4. DESCRIPTIVE NOTES: If appropriate, enter the type of report, e.g., interim, progress, summary, annual, or final. Give the inclusive dates when a specific reporting period is covered.

5. AUTHOR(S): Enter the name(s) of author(s) as shown on or in the report. Enter last name, first name, middle initial. If military, show rank and branch of service. The name of the principal author is an absolute minimum requirement.

6. REPORT DATE: Enter the date of the report as day, month, year, or month, year. If more than one date appears on the report, use date of publication.

7a. TOTAL NUMBER OF PAGES: The total page count should follow normal pagination procedures, i.e., enter the number of pages containing information.

7b. NUMBER OF REFERENCES: Enter the total number of references cited in the report.

8a. CONTRACT OR GRANT NUMBER: If appropriate, enter the applicable number of the contract or grant under which the report was written.

8b, 8c, & 8d. PROJECT NUMBER: Enter the appropriate military department identification, such as project number, subproject number, system numbers, task number, etc.

9a. ORIGINATOR'S REPORT NUMBER(S): Enter the official report number by which the document will be identified and controlled by the originating activity. This number must be unique to this report.

9b. OTHER REPORT NUMBER(S): If the report has been assigned any other report numbers (*either by the originator or by the sponsor*), also enter this number(s).

10. AVAILABILITY/LIMITATION NOTICES: Enter any limitations on further dissemination of the report, other than those imposed by security classification, using standard statements such as:

(1) "Qualified requesters may obtain copies of this report from DDC."

(2) "Foreign announcement and dissemination of this report by DDC is not authorized."

(3) "U. S. Government agencies may obtain copies of this report directly from DDC. Other qualified DDC users shall request through ________________."

(4) "U. S. military agencies may obtain copies of this report directly from DDC. Other qualified users shall request through ________________."

(5) "All distribution of this report is controlled. Qualified DDC users shall request through ________________."

If the report has been furnished to the Office of Technical Services, Department of Commerce, for sale to the public, indicate this fact and enter the price, if known.

11. SUPPLEMENTARY NOTES: Use for additional explanatory notes.

12. SPONSORING MILITARY ACTIVITY: Enter the name of the departmental project office or laboratory sponsoring (*paying for*) the research and development. Include address.

13. ABSTRACT: Enter an abstract giving a brief and factual summary of the document indicative of the report, even though it may also appear elsewhere in the body of the technical report. If additional space is required, a continuation sheet shall be attached.

It is highly desirable that the abstract of classified reports be unclassified. Each paragraph of the abstract shall end with an indication of the military security classification of the information in the paragraph, represented as (*TS*), (*S*), (*C*), or (*U*).

There is no limitation on the length of the abstract. However, the suggested length is from 150 to 225 words.

14. KEY WORDS: Key words are technically meaningful terms or short phrases that characterize a report and may be used as index entries for cataloging the report. Key words must be selected so that no security classification is required. Identifiers, such as equipment model designation, trade name, military project code name, geographic location, may be used as key words but will be followed by an indication of technical context. The assignment of links, rules, and weights is optional.

DD FORM 1 JAN 64 1473 (BACK)

Unclassified
Security Classification